https://doi.org/10.1093/plphys/kiac427 PLANT PHYSIOLOGY 2022: 00: 1–19

Plant Physiology®

Research Article

Formin protein DRT1 affects gross morphology and chloroplast relocation in rice

Yanli Zhang [1,2], Guojun Dong [3], Limin Wu [1], Xuewen Wang [4], Fei Chen [1], Erhui Xiong [1], Guosheng Xiong [5], Yihua Zhou [6], Zhaosheng Kong [7], Ying Fu [8], Dali Zeng [3], Dianrong Ma,[2] Qian Qian [3,*] and Yanchun Yu [1,9,*]

1 College of Life and Environmental Sciences, Hangzhou Normal University, Hangzhou, 310036, China
2 Rice Research Institute, Shenyang Agricultural University, Shenyang, 110866, China
3 State Key Laboratory for Rice Biology, China National Rice Research Institute, Hangzhou, 310006, China
4 Institute of Plant Breeding, Genetics, and Genomics, University of Georgia, Athens, Georgia, 30601, USA
5 Institute of Agricultural Genomics, Chinese Academy of Agricultural Sciences, Shenzhen, 100018, China
6 State Key Laboratory of Plant Genomics, Institute of Genetics and Developmental Biology, Chinese Academy of Sciences, Beijing, 100101, China
7 State Key Laboratory of Plant Genomics, Institute of Microbiology, Chinese Academy of Sciences, Beijing, 100101, China
8 State Key Laboratory of Plant Physiology and Biochemistry, College of Biological Sciences, China Agricultural University, Beijing, 100193, China
9 Zhejiang Provincial Key Laboratory for Genetic Improvement and Quality Control of Medicinal Plants, Hangzhou Normal University, Hangzhou, 310036, China

*Author for correspondence: ycyu@hznu.edu.cn (Y.Y.), qianqian188@hotmail.com (Q.Q.)
These authors contributed equally to this work (Y.Z., G.D., and L.W.)
Y.Y., Q.Q., D.M., and Y.Zhang designed the research. Y.Zhang, L.W., F.C., E.X., and G.D. performed the experiments. Z.K. and D.Z. contributed new reagents and analytic tools. Y.F., G.X., and Y.Zhang analyzed the data. Y.Y., Q.Q., Y.Zhou, and Y.Zhang wrote the draft manuscript. X.W. and Y.Y. revised the manuscript.
The author responsible for distribution of materials integral to the findings presented in this article in accordance with the policy described in the Instructions for Authors (https://academic.oup.com/plphys/pages/general-instructions) is: Yanchun Yu (ycyu@hznu.edu.cn).

Abstract

Plant height and tiller number are two major factors determining plant architecture and yield. However, in rice (*Oryza sativa*), the regulatory mechanism of plant architecture remains to be elucidated. Here, we reported a recessive rice mutant presenting dwarf and reduced tillering phenotypes (*drt1*). Map-based cloning revealed that the phenotypes are caused by a single point mutation in DRT1, which encodes the Class I formin protein *O. sativa* formin homolog 13 (OsFH13), binds with F-actin, and promotes actin polymerization for microfilament organization. DRT1 protein localized on the plasma membrane (PM) and chloroplast (CP) outer envelope. DRT1 interacted with rice phototropin 2 (OsPHOT2), and the interaction was interrupted in *drt1*. Upon blue light stimulus, PM localized DRT1 and OsPHOT2 were translocated onto the CP membrane. Moreover, deficiency of DRT1 reduced OsPHOT2 internalization and OsPHOT2-mediated CP relocation. Our study suggests that rice formin protein DRT1/OsFH13 is necessary for plant morphology and CP relocation by modulating the actin-associated cytoskeleton network.

Received June 07, 2022. Accepted August 21, 2022. Advance access publication September 14, 2022

Introduction

Plant architecture is a complex trait, controlled by plant height, tiller number, tiller angle, etc. (Wang and Li, 2008). Microfilament and microtubule-based cytoskeletal systems affect the establishment of plant architecture (Wang et al., 2012) via participating in many cellular processes, including cell growth and polarity establishment (Xie and Miao, 2021), cell division (Wang et al., 2012), cytoplasmic streaming (Wang et al., 2020), organelle movement (Perico and Sparkes, 2018), and cellular signaling (Lian et al., 2021).

Formins are cytoskeletal regulators with two conserved formin homologous domains, FH1 (Pro-rich domain) and FH2 (Goode and Eck, 2007). FH1 domain interacts with the small protein profilin and other proteins containing SH3 and WWP/WW domains (Cvrckova, 2013). FH2 domain has the actin-binding site that nucleates actin assembly and binds to the barded end of the actin filament (Kovar and Pollard, 2004). Plant formins are multigene families and can be divided into two major groups: Classes I and II. Most Class I formins contain a putative N-terminal signal peptide and a transmembrane domain. There is a GOE domain between the transmembrane domain and the FH1 domain for some formins. For example, there is a GOE domain in the Arabidopsis (*Arabidopsis thaliana*) AtFH4 protein, which can be connected directly with microtubules (Deeks et al., 2010). Some Class II formins carry a PTEN (N-terminal phosphatase and tensin) domain besides the conserved FH1 and FH2 domains (Grunt et al., 2008). Most of the studies focused on their biochemical characteristics, which have shown that plant formins have varying activities with respect to actin nucleation, bundling, severing, and microtubule binding (Fu et al., 2005). A number of Class I formins, including AtFH1, AtFH3, AtFH5, and AtFH8, were reported to be microfilament regulators that affect the polarized growth of pollen tubes or root cells (Ingouff et al., 2005; Michelot et al., 2005; Yi et al., 2005; Michelot et al., 2006; Xue et al., 2011; Rosero et al., 2017). Class I formins were also reported as microtubule regulators (Deeks et al., 2010; Rosero et al., 2016; Cifrova et al., 2020). However, some different functions of formins were gradually discovered, for example, AtFH1 in endomembrane reorganization (Oulehlova et al., 2019); AtFH4 can co-align membranes with actin and microtubule (Deeks et al., 2005); AtFH6 was reported to be involved in the isotropic growth of hypertrophied feeding cells via the reorganization of the actin cytoskeleton (Favery et al., 2004). Recent studies also found that AtFH6 was gradually recruited and condensed by remorin upon pattern-triggered immunity activation in lipid bilayers, consequently increasing actin nucleation in a time-dependent manner postinfection (Ma et al., 2021). Rice (*Oryza sativa*) formin proteins OsFH1 and OsFH15 play a substantial role in root hair elongation and grain-size regulation, respectively (Huang et al., 2013; Sun et al., 2017). Unlike most Class I formins, the Class II formins AtFH14, AtFH16, AtFH19, and OsFH5 are primarily involved in plant cell division and plant morphology (Li et al., 2011; Yang et al., 2011; Zhang et al., 2011; Zheng et al., 2012; Wang et al., 2013). AtFH13 and OsFH5 are essential for the spatial regulation of pollen tube growth (Li et al., 2018; Kollarova et al., 2021). Despite recent substantial progress toward understanding the cellular and molecular functions of a subset of Arabidopsis and rice formins, it remains a major challenge to explore the other potential physiological functions in plants, particularly in rice.

Light is essential for photosynthesis and plant growth (Liu et al., 2019); however, plants frequently get exposed to excess light, which negatively impacts photosynthetic activity and ultimately hampers plant growth and yield (Nishiyama and Murata, 2014). Chloroplast (CP) avoidance movement is evident in high light conditions where CPs move from the cell surface to the sidewalls of the cell. This movement reduces the amount of light absorbed, causing less photodamage (Kasahara et al., 2002). Although the phenomenon is widely observed in various plant species (Wada, 2013; Suetsugu et al., 2017), previous findings have suggested that some plants, such as rice, might not exhibit CP movement upon high light irradiation (Inoue and Shibata, 1973). However, the investigations performed by Kihara and his colleagues revealed that all examined *Oryza* species showed the blue-light-induced CP movements (Kihara et al., 2020). Arabidopsis phototropins (AtPHOT1 and AtPHOT2) are crucial in such CP movement, and their trafficking network plays a role in this response (Jarillo et al., 2001; Kong et al., 2013; Yang et al., 2019). Recently, the observations by Sakata et al. in gemma cells of *Marchantia polymorpha* revealed that relocation of MpPHOT to the CP periphery is critical for the initiation of CP movement (Sakata et al., 2019). The conserved ortholog of PHOTOTROPIN2 (PHOT2) has been identified as a regulatory element for CP avoidance in cotton (*Gossypium hirsutum*) and was examined cytoplasmic motility in the transient expression system upon high blue light irradiation (Shang et al., 2019). Besides phototropins, other factors that mediate CP mobility have also recently been identified. The coiled-coil domain protein CP UNUSUAL POSITIONING1 is targeted to the CP and bridges the plasma membrane (PM) with CP actin filaments to regulate CP mobility (Schmidt von Braun and Schleiff, 2008). Two kinesin-like proteins, KINESIN LIKE PROTEIN FOR ACTIN BASED CP MOVEMENT 1 and 2 (KAC1 and KAC2), exhibited actin-binding activity. KAC1 and KAC2-mediated CP-actin filaments regulate CP relocation (Suetsugu et al., 2010, 2012). The involvement of the actin cytoskeleton in CP movement had already been inferred by the effects of the anti-actin drugs cytochalasin B and D and latrunculin B (Kong and Wada, 2011). In Arabidopsis, disruption of actin filaments by Latrunculin B induced aberrant CP aggregation, suggesting that rapid reorganization of actin filaments contributes to the intracellular positioning of CPs (Kandasamy and Meagher, 1999). PSTAIRE-type cyclin-dependent kinase CDKA in the moss *Physcomitrium (Physcomitrella) patens* and its homolog in *A. thaliana* control light-induced tropisms and CP movements by probably influencing the cytoskeleton organization (Bao et al., 2022). Although the

complement of photoreceptors and multiple downstream signaling components have been uncovered, the molecular mechanism of how actin filaments are involved in phototropin relocation is still obscure.

In this study, we reported the identification of a rice mutant presenting dwarf and reduced tillering phenotypes (*drt1*). The *drt1* phenotypes are caused by mutated *DRT1* encoding a formin protein OsFH13. The deficiency of DRT1 impaired longitudinal actin filament organization. Further analyses found that DRT1 interacted with OsPHOT2 in CP relocation, which is affected by excessive light. Thus, DRT1 bridges the actin cytoskeleton and light signal transduction in rice.

Results

The *drt1* mutant displays pleiotropic phenotypes

To elucidate the molecular mechanism of rice development, we screened the population of ethyl methanesulfonate (EMS)-treated *Indica* variety SH527 to acquire mutants with altered architecture. Compared with the wild-type (WT) plant, the gross morphology of the *drt1* mutant plant was substantially changed, including reduced length of shoot, root, panicle, and grain and decreased tiller number (Figure 1, A–C and E). The mutant showed a dwarf phenotype in both vegetative and reproductive phases (Figure 1, A–B). The number of rachis branches and spikelets was reduced compared with the WT plant. The seeds of *drt1* were smaller with irregular shapes and were not well filled (Figure 1C). To determine whether the dwarfism phenotype of *drt1* was caused by cell division or cell elongation, we measured the cell length and width of the epidermal cells from *drt1* and WT leaf sheath. As shown in Figure 1D, the total number of cells in *drt1* in the same given region was increased, indicating that the length of cells in *drt1* was much shorter than that in WT. In contrast, the cells in *drt1* were much wider than in WT (Figure 1, D, F, and G). Measurements of root cells' size were significantly shorter in *drt1* than in WT (Supplemental Figure S1, A–E). In addition, the flower filaments were shorter than those of the WT (Supplemental Figure S1F), and fertility of some pollen grains was poorer in *drt1* than in the WT (Supplemental Figure S1G). In summary, DRT1 affects multiple developmental aspects in rice, which suggest an important role of DRT1 in development.

DRT1 encodes the Class I formin OsFH13

Our further genetic analysis showed that the *drt1* phenotype was controlled by a single recessive nuclear locus (Supplemental Table S1). Map-based cloning narrowed the mapping region to a 74.3-Kb DNA segment with 13 open reading frames (ORFs; Figure 2A). After DNA sequencing of these ORFs, the *drt1* mutation was identified as a C/T missense mutation at 610 bp downstream of the start codon of gene LOC_Os07g39920, which converted amino acid 204 from proline to serine (refer to as P204S thereafter; Figure 2, B and C). Sequence comparison revealed that DRT1 had been referred to as OsFH13, a Class I formin (Cvrckova et al., 2004; Grunt et al., 2008). The C-terminus of DRT1 contains two conserved domains, called FH1 and FH2, and the P204 residue is in the FH1 domain, which is evolutionarily conserved among maize (*Zea mays*), *Brachypodium distachyon*, and rice species (Supplemental Figure S2). One hypothesis is that the effect of the mutation is due to different effects of Pro and Ser on the protein backbone conformation.

To verify that the phenotype is caused by *DRT1*, we conducted complementation analysis to introduce the full-length genomic fragment of *DRT1* from WT into *drt1* (Figure 2D), and found that all phenotypes of *drt1*, including dwarf, small panicle shape, and other agronomic characters, were rescued in complementation plants (Figure 2E; Supplemental Table S2). To further verify the deficiency of DRT1 was responsible for the defective phenotypes, we also generated two more *drt1* alleles using the CRISPR/Cas9 method. *drt1-2* and *drt1-3* had deleted AT and GA nucleotides in the first exon, respectively (Supplemental Figure S3A). To determine whether these alterations impaired protein translation, we produced a DRT1-specific antibody and performed immunoblot analysis with total proteins from *drt1-2* and *drt1-3*. The results revealed that DRT1 protein was depleted in *drt1-2* and *drt1-3* (Supplemental Figure S3B). Concordantly, *drt1-2* and *drt1-3* exhibited more severe developmental defects than *drt1*, including a greater reduction in plant height, tiller number (Supplemental Figure S3C; Supplemental Table S3), and cell length (Supplemental Figure S3, D–E). We, therefore, concluded that the mutation in *DRT1/OsFH13* was responsible for the *drt1* phenotypes.

The expression pattern of DRT1

We examined the transcripts of *DRT1* with reverse transcription-quantitative PCR (RT-qPCR) and found that gene *DRT1* was transcribed in all the five organs tested from vegetative to reproductive stages. The *DRT1* showed maximal expression in leaf among all tested organs followed by leaf sheath, stem, and root, and low expression in panicle (Supplemental Figure S4A). We also checked the DRT1 protein abundance with multiple organs by immunoblot analysis. As shown in Supplemental Figure S4B, the content of DRT1 protein was the highest in leaves, and the accumulation amount was slightly less in leaf sheath and stem, concordant with RT-qPCR results. To further examine the DRT1 expression pattern, the GUS reporter gene driven by the DRT1 promoter was introduced into WT plant, and the histochemical staining of transgenic plants validated that the DRT1 was universally expressed. In etiolated seedlings, DRT1 expression was detected in both roots and coleoptiles. In root apexes, GUS signals were observed in root caps. A cross-section of the leaves indicated that DRT1 was expressed in the vascular bundles (Supplemental Figure S4, C–E) and the mesophyll cells of expanded leaves (Supplemental Figure S4, F–H).

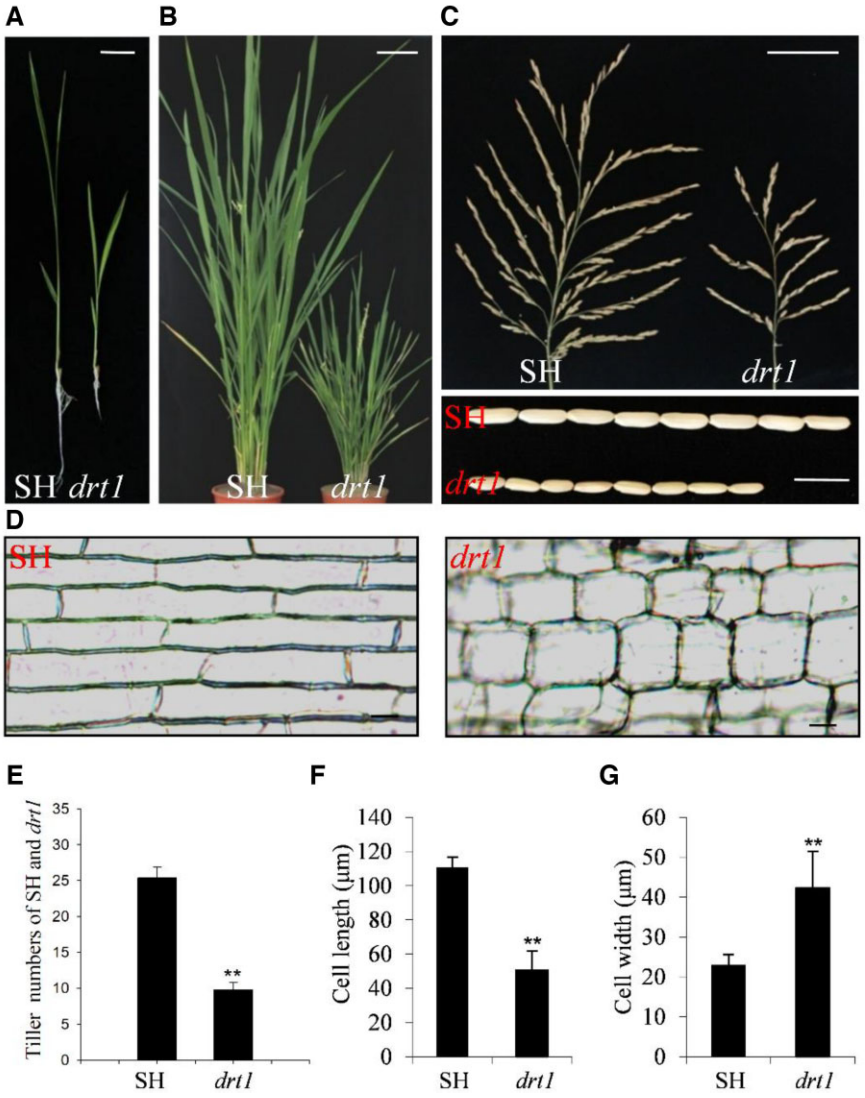

Figure 1 Phenotypes of WT and *drt1* mutant. A, 20-d-old seedlings of the WT (SH) and *drt1*. Scale bar = 5 cm. B, Rice plants at heading stage. Scale bar = 10 cm. C, Panicle rachis and seeds of WT and *drt1* plants. Scale bar = 10 cm for panicle, Scale bar = 1 cm for seeds. D, Cells of leaf sheath from 12-d-old WT and *drt1* seedlings. Scale bar = 20 μm. E, Tiller numbers of WT and *drt1* mutant at heading stage. F, Cell length of WT and *drt1* mutant. G, Cell width of WT and *drt1* mutant. Statistical analysis was performed by *t* test. Means ± SD were given in (E; $n = 20$), F ($n = 30$), and G ($n = 30$). $^{**}P < 0.01$.

DRT1 is required for microfilament organization

Considering that DRT1 encodes a putative formin protein (Figure 2; Supplemental Figure S2), we hypothesized whether DRT1 affects the organization of the cytoskeleton. We stained F-actin with Alexa Fluor 488-phalloidin, a dye widely used for detecting F-actin in pollen grains and root tips (Zhang et al., 2011). Under the same staining and observation conditions with confocal laser microscopy, the average fluorescence intensity in WT cells (Figure 3, A and E) was significantly stronger than in *drt1* mutant cells (Figure 3, B, F, I, and J), indicating that F-actin abundance was reduced in *drt1*. Second, in contrast to the precisely organized filaments longitudinally in the cortical cells of the root elongation region of WT (Figure 3C), only a few longitudinal actin cables were detected in *drt1* cells even when the signal detection settings had been improved considerably, and more transverse filaments were shown in the cells (Figure 3D). Thirdly, cortical cells in the root elongation zone of *drt1* were short in length and had a deformed shape compared to those in WT (Figure 3, C and D), which may explain the short phenotype of roots. We found the filaments in root hair in *drt1* mutant displayed scattered and dispersed, rather than fascicular and linear in the WT (Figure 3, G and H). Moreover, *drt1-2* and *drt1-3* showed similar or even more severe microfilament polymerization and organization defects than *drt1* mutant, such as discontinuous and dispersive actin filaments (Supplemental Figure S5, D and E). More importantly, all these defects of filament organization in *drt1* were all rescued in complemented plants (Supplemental Figure S5, A–C). These observations indicate that DRT1 affects actin organization and filament network formation in rice.

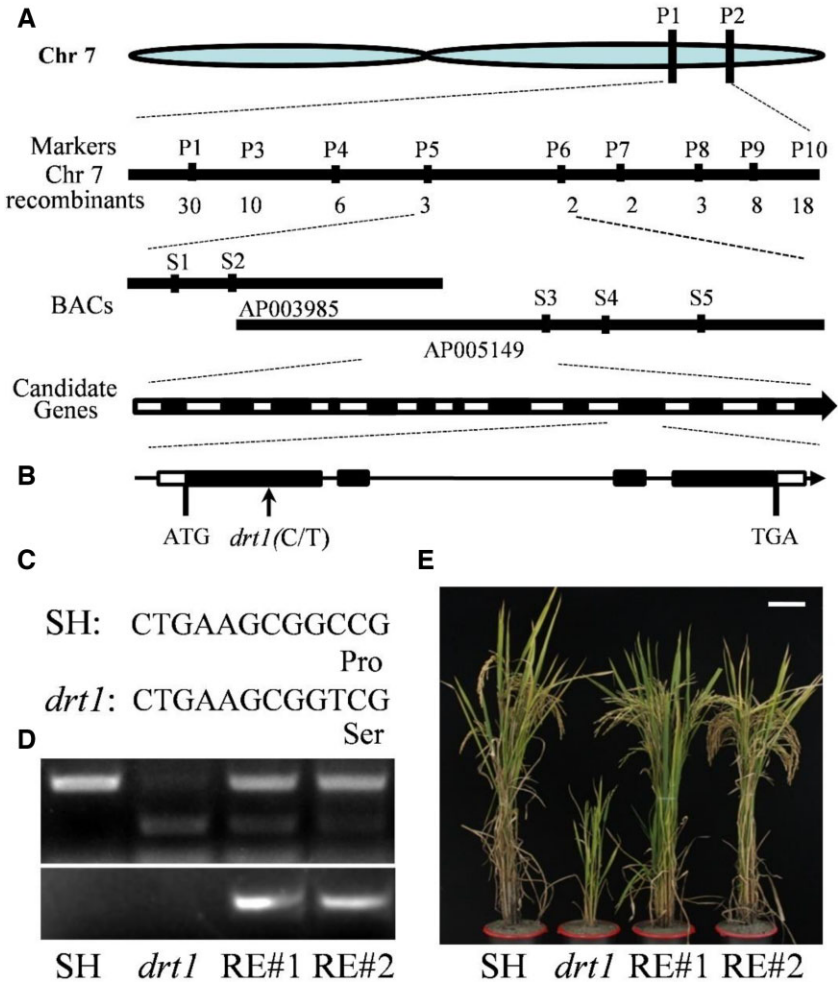

Figure 2 Map-based cloning of *DRT1* gene and complementation of the *drt1* mutant. A, *DRT1* was mapped primarily to the end of rice chromosome 7 between markers P1 and P2, and then narrowed to a 74.3 Kb region. B, Amplification of relevant DNA fragments and sequence comparison revealed that the *drt1* alleles resulted from a single base substitution (C to T) in the first exon of the *DRT1* gene. C, Change of amino acid residue from Pro to Ser at residue 204 in *drt1* mutant. D, Confirmation of the transgenic *DRT1* construct into *drt1* mutant background. The upper panel indicated materials background confirmed by restriction enzyme (Hpy188I) digestion; the Lower panel indicated the confirmation of transgenic lines. E, Phenotypic complementation of the *drt1* mutant by the introduction of the *DRT1* gene. Scale bar = 10 cm. SH, wild-type; RE, complementation plant.

DRT1 directly binds to microfilaments and promotes actin polymerization

Formins have been reported to regulate actin dynamics (Goode and Eck, 2007; Chang et al., 2021). To test whether DRT1 presented the actin-binding activity, we performed an actin-binding assay with purified DRT1. Unfortunately, we failed to purify the full length of DRT1 after several attempts. The FH1FH2 fragment of formin was the essentially functional domain in bundling actin filaments (Zhang et al., 2011; Wang et al., 2013); Thus, we then used the FH1FH2 fragment to do an actin polymerization assay. We mixed the GFP-HIS and FH1FH2-GFP-HIS proteins with rabbit muscle actin for in vitro binding assay, followed by protein gel blot analysis. HIS antibody was used to detect the quality of the purified proteins. As shown in Figure 4A, actin protein was detected with FH1FH2-GFP-HIS, whereas it was not in GFP-HIS control, indicating that DRT1 bound to actin in vitro. To visually detect whether FH1FH2 could bind to actin filaments, the G-actin (Figure 4, B1–B4) and actin filaments (Figure 4, B5–B8) were incubated with FH1FH2 protein, respectively, and the results revealed that both of them co-localized with FH1FH2. We further performed the ultraviolet spectrophotometer experiment following the instruction by Ren et al. (1997) to determine whether DRT1 could regulate actin polymerization. As shown in Figure 4C, after 2 h of polymerization, the microfilaments and actin monomers in the system were stable; the polymerization and depolymerization reached a relatively dynamic balance (blue). However, with FH1FH2-GFP-His added, the polymerization was promoted in a concentration-dependent manner (gray

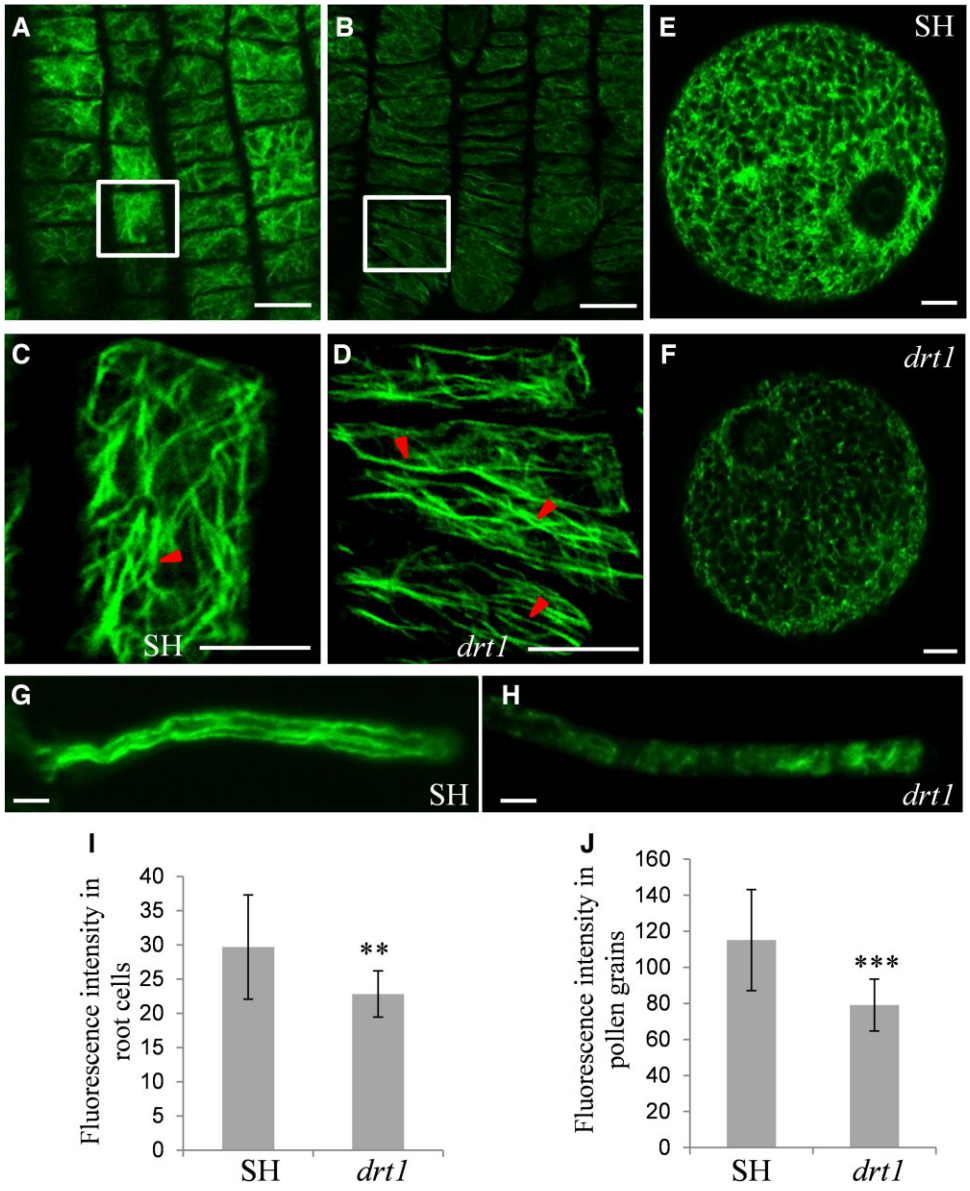

Figure 3 *drt1* mutant defective in actin microfilament networks. A–D, Actin filaments of cells from the root elongation zone of 4-d-old rice seedlings, stained by Alexa Fluor 488-phalloidin. A, WT cells. Scale bar = 10 μm. B, *drt1* cells. Scale bar = 10 μm. C, A close-up of the boxed region in (A). Scale bar = 2 μm. D, A close-up of the boxed region in (B). Red triangles indicate the organization in WT and *drt1* mutant. Scale bar = 2 μm. E and F, F-actin organization in pollen grains of WT and the *drt1* mutant. Scale bar = 5 μm. G and H, F-actin organization in root hair of WT and the *drt1* mutant. Scale bar = 10 μm. I, The average fluorescence pixel intensity of WT and *drt1* root cells. J, The average pixel intensities in each pollen grain in the WT and *drt1* mutant. Statistical analysis was performed by *t* test. Means ± SD were given in (I; $n = 30$) and (J; $n = 20$). $^{**}P < 0.01$, $^{***}P < 0.001$.

and yellow). Together, these results suggested that DRT1 was involved in actin binding and polymerization.

DRT1 is positioned in the PM and CP membrane

To determine the subcellular localization of DRT1, the construct pMDC83-35S:: DRT1-GFP was introduced into rice protoplasts via polyethylene glycol (PEG)-mediated transformation and *Nicotiana benthamiana* by *Agrobacterium tumefaciens*-mediated injection. We found that the free GFP signal was ubiquitously distributed in cells with the 35S::GFP vector control (Supplemental Figure S6, C and D). In contrast, the DRT1-GFP fluorescence is observed in the surface of the cells or the cytoplasm (Figure 5, A and B; Supplemental Figure S6, A and B). Given that DRT1 has a typical transmembrane domain (Supplemental Figure S2), and the cytoplasmic GFP fluorescence is overlapped with chlorophyll autofluorescence, we assumed DRT1 protein is located on the PM or CP. We then isolated proteins from the PM and CP to perform immunoblot with organelle-specific antibodies as a control to validate that hypothesis. The results showed that DRT1 appeared both in the PM and CP components

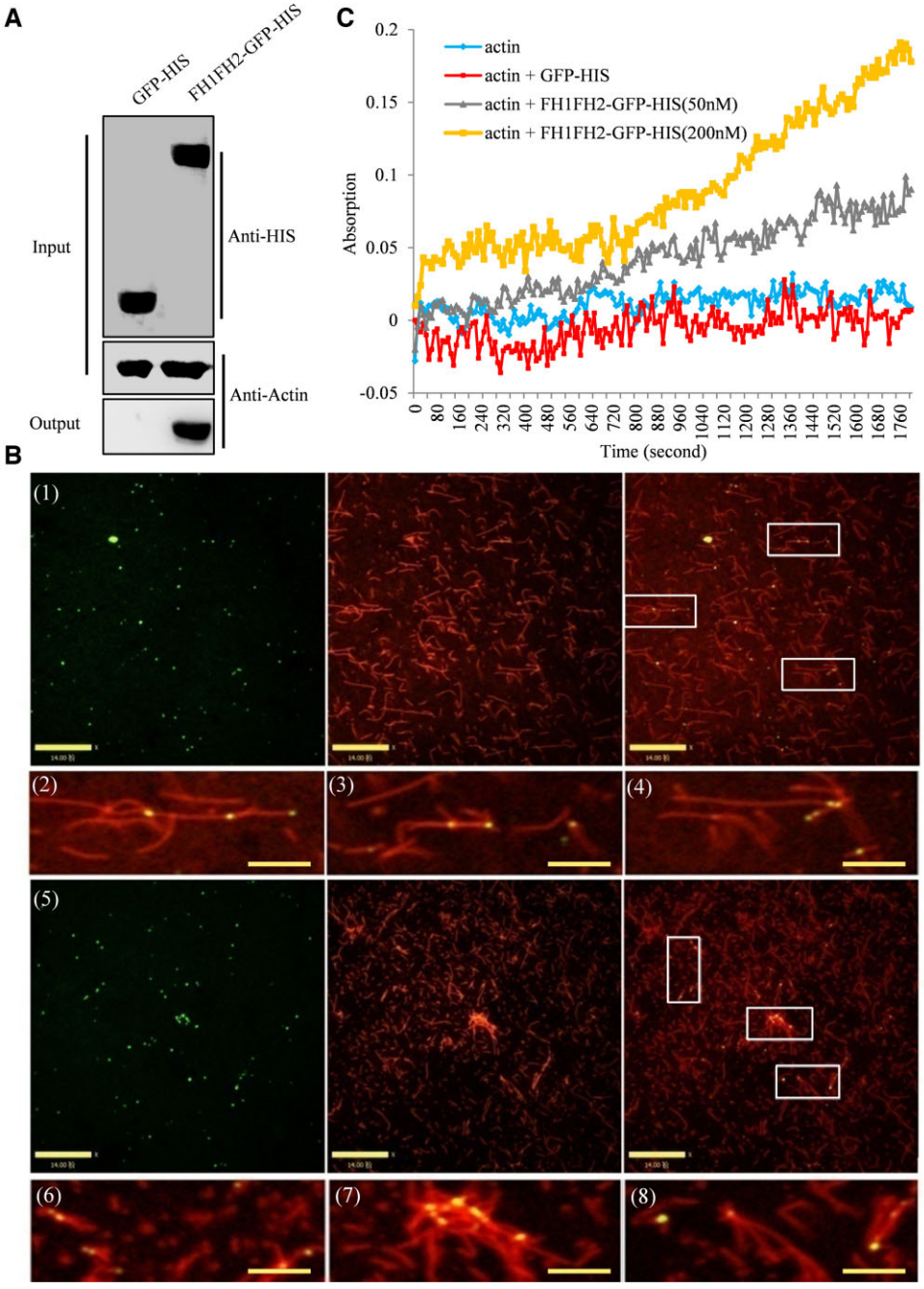

Figure 4 In vitro binding and actin polymerization effect of DRT1FH1FH2-GFP-HIS. A, In vitro binding of DRT1FH1FH2-GFP-HIS to actin. GFP-HIS (lane 1) and DRT1FH1FH2-GFP-HIS (lane 2) were subjected to in vitro binding assay to actin and then analyzed by protein gel blotting using an anti-Actin antibody. B, 3 μM G-actin incubated with 1 μM DRT1FH1FH2-GFP (1). (2–4) Enlarged view of the three regions marked in (1). The 3-μM actin filament incubated with 1 μM DRT1FH1FH2-GFP (5). (6–8) Enlarged view of the three regions marked in (5). Scale bar in (1, 5) = 5 μm; Scale bar in (2, 3, 4, 6, 7, and 8) = 0.2 μm. C, Ultraviolet absorption spectra of actin polymerization. About 4 μmol/L actin only (third curve from top to bottom); 4 μmol/L actin + 50 nmol/L GFP-HIS (fourth curve from top to bottom); 4 μmol/L actin + 50 nmol/L DRT1FH1FH2-GFP-HIS (second curve from top to bottom); 4 μmol/L actin + 200 nmol/L DRT1FH1FH2-GFP-HIS (first curve from top to bottom).

(Figure 5C). To further assess the sub-organelle localization of DRT1 within the CP, we separated the thylakoid membrane, stroma, and envelope fractions using density gradient ultra-centrifugation, followed by immunoblot analysis. As shown in Figure 5D, DRT1 was detected in the Tic110 fraction, a well-established envelope marker, indicating the localization of DRT1 in the CP envelope. Protease sensitivity assays were applied to detect the CP protein position (Kong et al., 2013). While both the inner envelope protein Tic110 and outer envelope protein Toc75 were resistant to protease, consistent with their deeply embedded positions in the membrane, DRT1 protein was sensitive to the protease thermolysin (Figure 5E), suggesting that it is peripherally associated with the CP outer envelope.

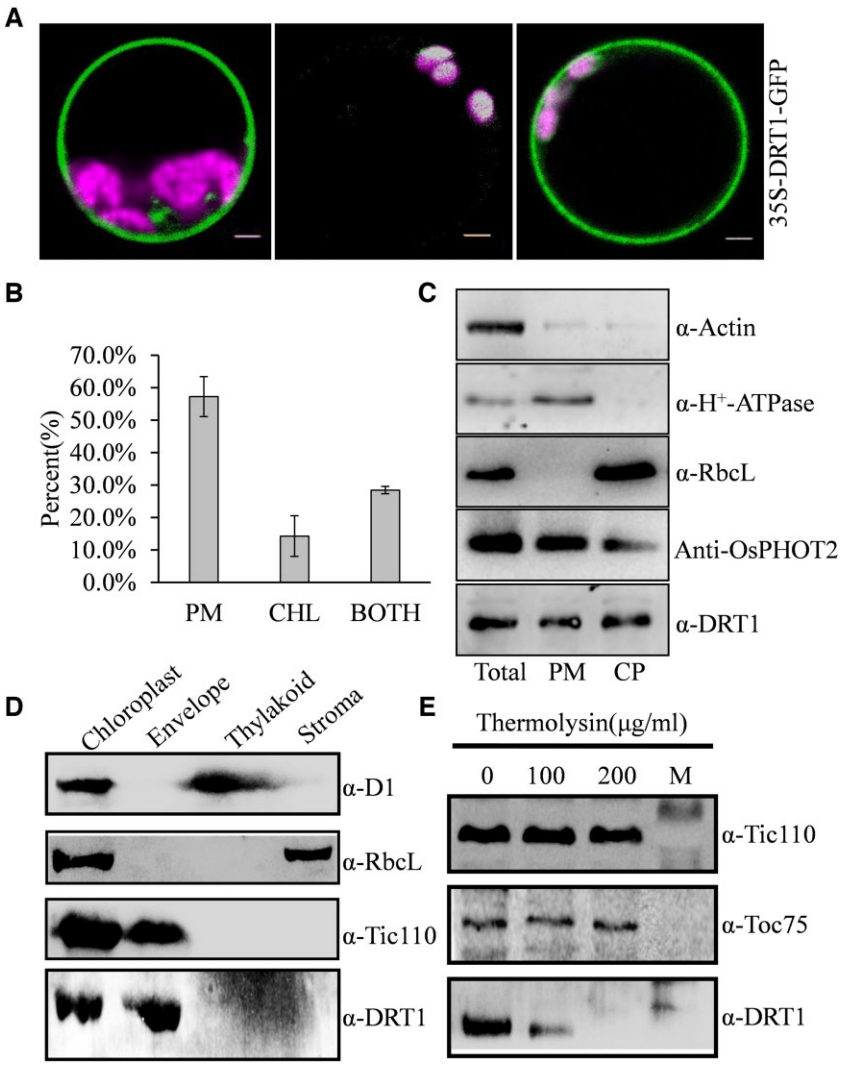

Figure 5 DRT1 relocates from the PM to the CP membrane. A, DRT1-GFP fusion constructs were transiently expressed in rice protoplasts for subcellular localization analysis. Three patterns of DRT1-GFP signal were observed: at the PM, CPs, and in both locations. Green fluorescence shows GFP; red fluorescence indicates CP autofluorescence, and yellow fluorescence indicates images merged with the two types of fluorescence. Scale bar = 2 μm. B, Quantification of cells that contained PM-localized GFP signal, CP (CHL)-localized signal or signal in both locations (BOTH) in rice protoplasts transfected with 35S::DRT1-GFP. Values are presented as means ± SD (n = 30). C, Subcellular localization of the DRT1 protein by immunoblot analysis. Total protein, PM protein, and CP protein were isolated from WT leaves. Immunoblot analysis was performed by using antibodies against Actin (total protein marker), RbcL (CP marker), H + -ATPase (PM marker), and DRT1. D, Sub-organelle localization of the DRT1 protein in the CP. Intact CPs were isolated from WT leaves and separated into envelope, thylakoid, and stroma fractions. Immunoblot analysis was performed by using antibodies against D1 (thylakoid marker), RbcL (stroma marker), Tic110 (envelope marker), and DRT1. E, Intact CPs were isolated from WT leaves and then treated with 0, 100, or 200 μg/mL thermolysin. Immunoblot analysis was performed using antibodies against Tic110 (an inner envelope protein), Toc75 (an outer envelope protein deeply embedded in the membrane), and DRT1.

DRT1 physically interacts with OsPHOT2

To further explore the function of DRT1, a yeast two-hybrid assay was utilized to isolate interactive proteins. OsPHOT2 (LOC_Os04g23890), a blue light receptor, was identified. Further examination revealed that OsPHOT2 and DRT1 could interact directly and that the DRT1 P204S point mutation in the FH1 domain abolished their interaction (Figure 6, A and B). The consistent result was acquired by the firefly luciferase complementation imaging (LCI) assay (Figure 6C). We tested their interaction using a co-immunoprecipitation approach to determine whether DRT1 interacted with OsPHOT2 in vivo. For this purpose, we transiently co-expressed DRT1 fused with a GFP tag (DRT1-GFP) and OsPHOT2 fused with HA (OsPHOT2-HA) in *N. benthamiana* leaves. OsPHOT2-HA was co-immunoprecipitated when DRT1-GFP was pulled down from leaf extracts with an anti-GFP antibody and detected with an anti-OsPHOT2 antibody (Figure 6D). To further map the OsPHOT2-DRT1 interaction region, we tried to induce and purify various truncated proteins of DRT1 and OsPHOT2 to do a pull-down assay (Supplemental Figure S7). The pull-down assay revealed that the interaction happened between the DRT1

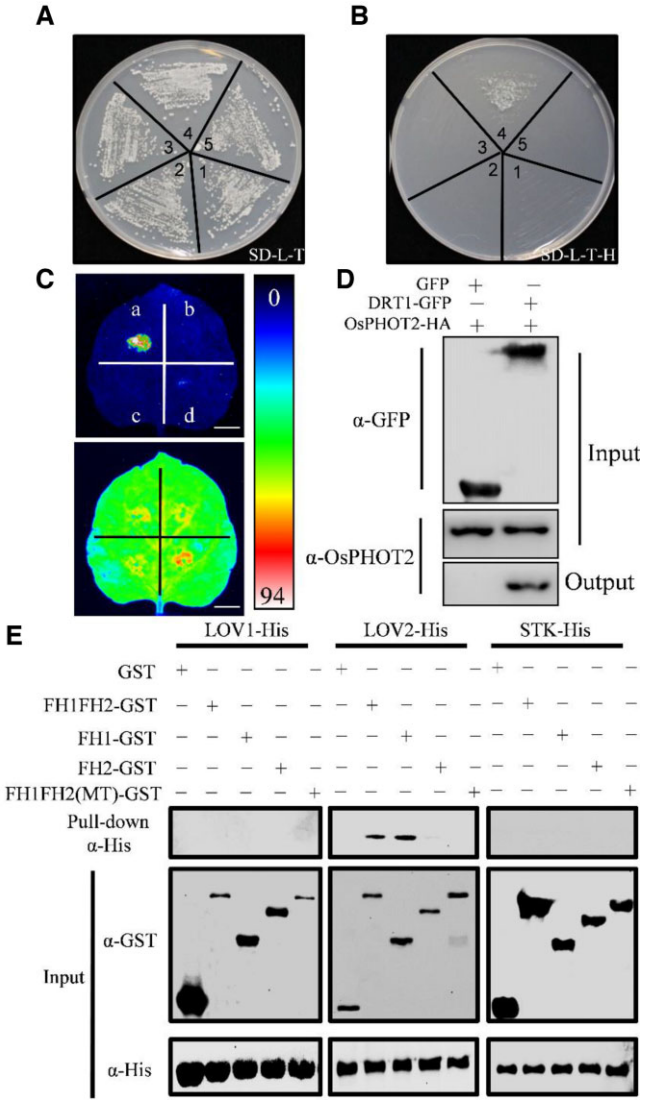

Figure 6 DRT1 physically interacts with OsPHOT2. A and B, Y2H showing that OsPHOT2 interacts with DRT1FH1FH2 (4) but not DRT1FH1FH2 (MT; 5). SD-L-T, SD medium without Leu and Trp; SD-L-T-H, SD medium without Trp, Leu, and His. pGBKT7 + pGADT7 (1), pGBKT7-DRT1FH1FH2 + pGADT7 (2) and pGBKT7 + pGADT7-OsPHOT2 (3) were used as negative controls. C, LCI assay showing the interaction between OsPHOT2 and DRT1FH1FH2. LUC image of *N. benthamiana* leaves co-infiltrated with Agrobacterium strains containing plasmids. (a) DRT1FH1FH2-LUC^N + LOV2-LUC^C, (b) DRT11 FH1FH2-LUC^N + LUC^C, (c) LUC^N + LOV2-LUC^C, (d) DRT1FH1FH2 (MT)-LUC^N + LOV2-LUC^C. Scale bar = 1 cm. D, In vivo interaction between OsPHOT2-HA and DRT1-GFP, revealed by the co-immunoprecipitation assay. After immunoprecipitation with anti-GFP (α-GFP), precipitated proteins were probed with an anti-OsPHOT2 antibody. E, In vitro pull-down assay of truncated recombinant protein of FH1FH2 and OsPHOT2. GST was used as a negative control.

FH1 domain and OsPHOT2 LOV2 domain, and the P204S attenuated its interaction with OsPHOT2 (Figure 6E). These results suggested that the DRT1 FH1 domain physically interacted with the OsPHOT2 LOV2 domain, and the P204 residue of DRT1 is critical for their interaction.

Osphot2 is defective in CP relocation

In Arabidopsis, AtPHOT2 mediates stomatal opening, leaf positioning and flattening, hypocotyl phototropism, and the CP photorelocation movement (Huala et al., 1997; Kinoshita et al., 2001). However, the physiological importance of OsPHOT2 is still obscure. To explore the physiological importance of OsPHOT2 and its functional interaction with DRT1, we generated *Osphot2* mutant in the NIP background using the CRISPR/Cas9 method, which inserted an additional "A" nucleotide at the first exon of the *OsPHOT2* CDS and presumably to produce a premature stop codon (Supplemental Figure S8, A and B). RT-qPCR analysis revealed that the transcriptional level of *OsPHOT2* was significantly decreased in the *Osphot2* mutant (Supplemental Figure S8C). Moreover, an immunoblot assay with a specific OsPHOT2 antibody found that OsPHOT2 protein was fully depleted in *Osphot2* mutants (Supplemental Figure S8D). However, unlike *drt1*, the *Osphot2* mutant lacked obvious developmental defects (Supplemental Figure S8E) and had only weak pale green leaves phenotype (Supplemental Figure S8F). That was consistent with the decreased chlorophyll content in the *Osphot2* mutant (Supplemental Figure S8G). We then determined the effect of light intensity on CP positioning in mesophyll cells using a confocal microscope with 24 h dark-adapted WT and *Osphot2* mutant plants irradiated with a low-fluence light (LL) or high-fluence light (HL) white light for 2 h. In cells of dark-adapted WT and *Osphot2* plants, most CPs were positioned at the bottoms of cells (Supplemental Figure S9A). Upon LL condition, most CPs were observed at the upper sides of mesophyll cells in both WT and *Osphot2* (Supplemental Figure S9A). In contrast, the distribution of *Osphot2* CPs was quite different from that in the WT under the HL condition. In WT, the CPs were along the anticlinal walls of mesophyll cells with HL stimulus as a CP avoidance response (Wada, 2013). In contrast, the CPs in *Osphot2* mutant still accumulated at the bottom of cells (Supplemental Figure S9A), indicating that the CPs in the mutant cells were less motivated upon high light stimulation than the WT. Our leaf cross sections assay acquired concordant results with confocal microscope observation (Supplemental Figure S9B). We performed a leaf transmittance assay to further detect precise distribution patterns of all CPs under different light conditions. In WT, weak blue light (50 μmol/m^2/s) induced a decrease in leaf transmittance, whereas intense blue light (360 μmol/m^2/s) induced an increase in leaf transmittance substantially as a result of the avoidance response. However, in the *Osphot2* mutant, the avoidance response was severely impaired, while the CP accumulation response was slightly affected (Supplemental Figure S9C). These investigations suggested that rice keeps the canonical OsPHOT2-mediated CP relocation response.

DRT1 affects OsPHOT2 internalization

Arabidopsis PHOT2 is localized in the PM and CP membrane, and the fine-tune regulation of its subcellular position is crucial for its functions (Ishishita et al., 2020). We next investigated whether OsPHOT2 is an intracellular mobility protein and whether its mobility is affected by DRT1. First, we transiently co-expressed DRT1-GFP and OsPHOT2-CFP fusion constructs in WT protoplasts and found that the fluorescences of DRT1-GFP and OsPHOT2-CFP were initially close to the margin of the cell. Upon light treatment, they gradually disappeared and there was an increased signal in the cytosol (Figure 7A). More importantly, the GFP and CFP signals overlapped and merged with CP auto-fluorescence after the 120 s blue light stimulus (Figure 7A). However, the PM-localized OsRAC protein (Ono et al., 2001) neither disappeared from PM nor appeared on CP with the same light treatment, even though OsRAC and DRT1 initially colocalized (Supplemental Figure S10B). Given that DRT1 is positioned in PM (Figure 5C) and it colocalizes with OsRAC (Supplemental Figure S10B), we hypothesized that the fluorescence of DRT1-GFP visualized on the margin of the cell is from PM.

LatB is an actin polymerization inhibitor, which had been applied to test the stability and/or turnover rate of actin filaments (Qu et al., 2020). We then pretreated protoplasts with LatB to see whether it affects the DRT1-GFP fluorescence alteration. We found the fluorescence reduction from the PM and increase on CPs by light stimulus had been greatly prevented by the LatB treatment (Supplemental Figure S10A). These data suggested that the diminished

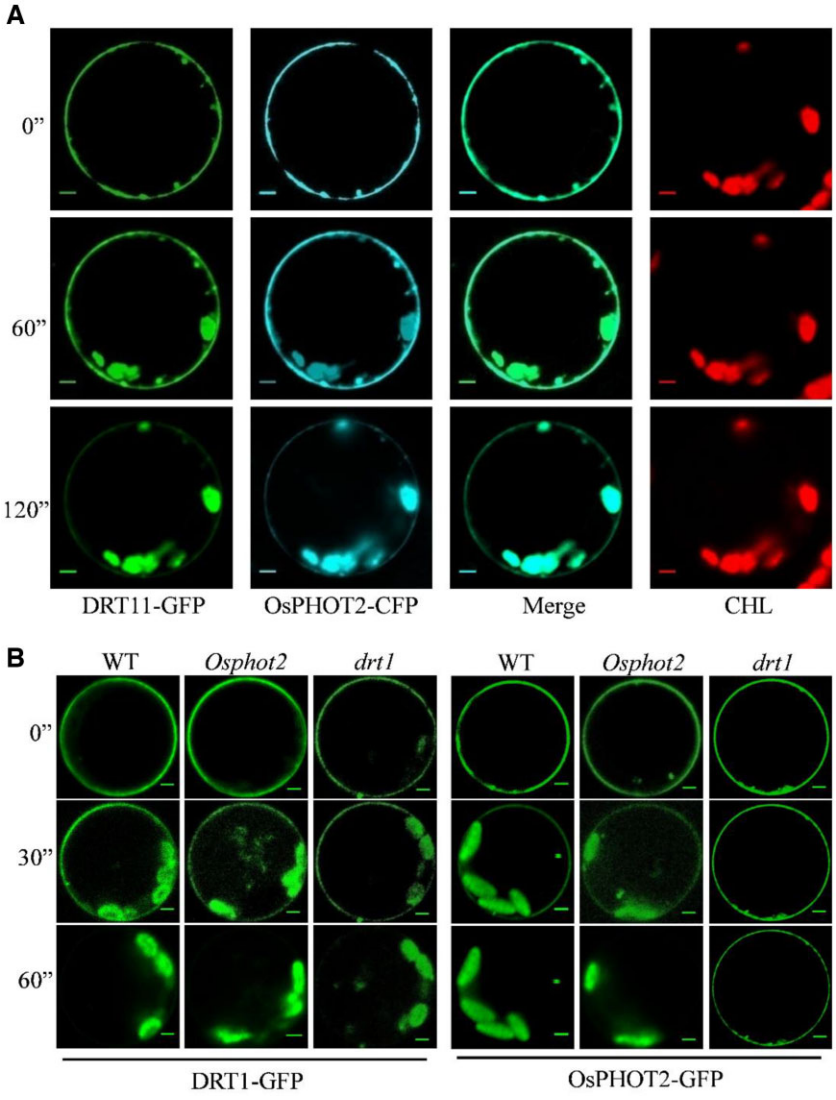

Figure 7 DRT1 regulates the intracellular distribution of OsPHOT2. A, Cells of protoplasts co-transfected with 35S::DRT1-GFP and 35S::OsPHOT2-CFP were visualized using a confocal laser scanning microscope after blue light stimulation for 0, 60, and 120 s. Scale bar = 2 μm. B, Transient expression using the DRT1-GFP fusion construct in WT, *Osphot2*, and *drt1* protoplasts (left). GFP fluorescence images were captured with a confocal laser scanning microscope after blue-light stimulation for 0, 30, and 60 s. Scale bar = 2 μm. Transient expression using the OsPHOT2-GFP fusion construct in WT, *Osphot2*, and *drt1* protoplasts (right). GFP fluorescence images were captured with a confocal laser scanning microscope after blue-light stimulation for 0, 30, and 60 s. Scale bar = 2 μm. CHL, CP autofluorescence.

DRT1 and OsPHOT2 proteins on the PM were caused by translocation, with no photobleaching. We then transformed OsPHOT2-GFP or DRT1-GFP plasmids into WT, *drt1*, and *Osphot2* protoplasts to observe whether DRT1 deficiency affects the relocation of OsPHOT2. The free GFP vector was used as the blank control. We found the GFP fluorescence from protoplasts expressing free GFP remained ubiquitously in cells under light stimulation (Supplemental Figure S11A). In contrast, DRT1-GFP and OsPHOT2-GFP presented a similar mobility feature in WT and *Osphot2* (Figure 7B); however, light stimulation failed to induce the shift of OsPHOT2-GFP signal from the PM to the CP in *drt1* protoplasts with the OsPHOT2-GFP (Figure 7B). A similar phenomenon was observed in the *drt1-2* mutant (Supplemental Figure S11B). More importantly, the impairment of OsPHOT2 shift in a mutant cell under blue light was rescued in represented RE#1 plant in the complementation analysis (Supplemental Figure S11C). These results indicated that DRT1 is required for OsPHOT2 internalization upon blue-light irradiation.

DRT1 participates in OsPHOT2-mediated CP relocation

To test whether DRT1 involves OsPHOT2-mediated light response, we first crossed *Osphot2* with *drt1-2* to produce *Osphot2/drt1-2* double mutant and found the gross morphology of *Osphot2/drt1-2* mimicked the *drt1-2* mutant (Figure 8A). For leaf transmittance assay, we irradiated WT, *drt1-2*, *Osphot2*, and *Osphot2/drt1-2* leaves with high or low light. Compared with the substantial impairment in avoidance response of *Osphot2* mutant, *drt1-2* and *Osphot2/drt1-2* plants were defective in both accumulation and avoidance responses (Figure 8B). We further analyzed CP photorelocation movement by histosection and confocal microscopy assay with the above four plants and acquired consistent results with the transmittance assay. The CPs in the *drt1-2* and *Osphot2/drt1-2* double mutant cells were less motivated upon light stimulation than *Osphot2* (Figure 8C; Supplemental Figure S12). These results support the possibility that DRT1 and OsPHOT2 work in the same pathway in mediating light response.

Discussion

DRT1 affects plant architecture

Plant architecture is important for crop yield improvement, and the process is tightly controlled by complicated developmental and environmental signals (Wang and Li, 2008). Previous research with QTL mapping and cloning has made substantial progress in the identification of associated genes, such as *Semi-Dwarf1*, *Dwarf1*, *BRASSINOSTEROID-INSENSITIVE1*, *MONOCULM 1*, *Tillering and Dwarf 1* and *Ideal Plant Architecture 1*, which regulate the plant height and tiller number (Wang and Li, 2008; Xu et al., 2012; Zhang et al., 2020). Recently, many plant structural cytoskeletal or cytoskeleton-associated genes have been identified in regulating plant architecture (Wang et al., 2012); however, the detailed molecular mechanism needs to be elucidated. In this study, we identified a dwarf and reduced tillering mutant *drt1*, which is determined by the deficiency of Class I formin OsFH13. Our investigations establish that the Class I formin can dramatically affect gross morphology in rice (Figure 1).

Formins have been recognized as actin-nucleating proteins that control the rate-limiting step of actin polymerization (Goode and Eck, 2007); however, the biological importance of formins in plant morphogenesis is relatively less investigated. In Arabidopsis and rice genomes, there are 21 and 16 putative formin genes, respectively, and most of them were reported to show their roles in the polarized growth of pollen tubes or root cells (Cvrckova et al., 2004). The less impairment on gross morphology for a single formin mutant happens due to overlapping expression patterns and functional redundancy among the formin isoforms (Zhang et al., 2011). Until 2011, studies demonstrated that mutation of a single type II formin (OsFH5) caused pleiotropic defects, including bent uppermost internode, dwarfism, wavy panicle rachis, and enhanced gravitropic response (Yang et al., 2011; Zhang et al., 2011). In addition, OsFH5 controls cell growth through the auxin-actin regulatory loop (Li et al., 2018). Recently, OsFH5 has been shown to control crown root angle in response to external phosphate and shoot gravitropism (Huang et al., 2018; Song et al., 2019). Another Class II formin, OsFH3, functions partially redundantly with OsFH5 in rice morphogenesis (Chang et al., 2021). OsFH1 (type I formin) was found to play a substantial role in root hair elongation in a growth condition-dependent manner. The *Osfh1* mutant exhibited root hair defects when roots were grown submerged in the solution, and the mutant produced normal root hairs in the air (Huang et al., 2013). DRT1/OsFH13 is a typical Class I formin containing an N-terminal transmembrane domain (Favery et al., 2004). *drt1* and *Osfh5* mutant present similar developmental phenotypes, including dwarf and reduced cell length (Figure 1). *Osfh5* has a deficiency in microtubule arrays in root cortical cells and pollen grains (Zhang et al., 2011). Our data showed that the reduced cell length of *drt1* is caused by an impaired microfilament cytoskeleton (Figure 3). However, we could not exclude the possibility that DRT1 affects cell expansion through impaired microtubule organization, like *Osfh5*. In addition, the *Osfh5* mutant had curled flag leaves and panicles, whereas these deficiencies did not present in *drt1*. Therefore, exploring the temporal and spatial expression regulation of all formin genes is necessary, especially DRT1 and OsFH5 in rice in the near future.

DRT1 is a putative traffic protein from the PM to the CP membrane

As we mentioned above, plant formins are divided into two different classes. Class I generally contains a transmembrane domain. Most of the identified Class I formins are indeed positioned on PM (Cheung and Wu, 2004; Favery et al., 2004; Deeks et al., 2010; Huang et al., 2013; Diao et al., 2018).

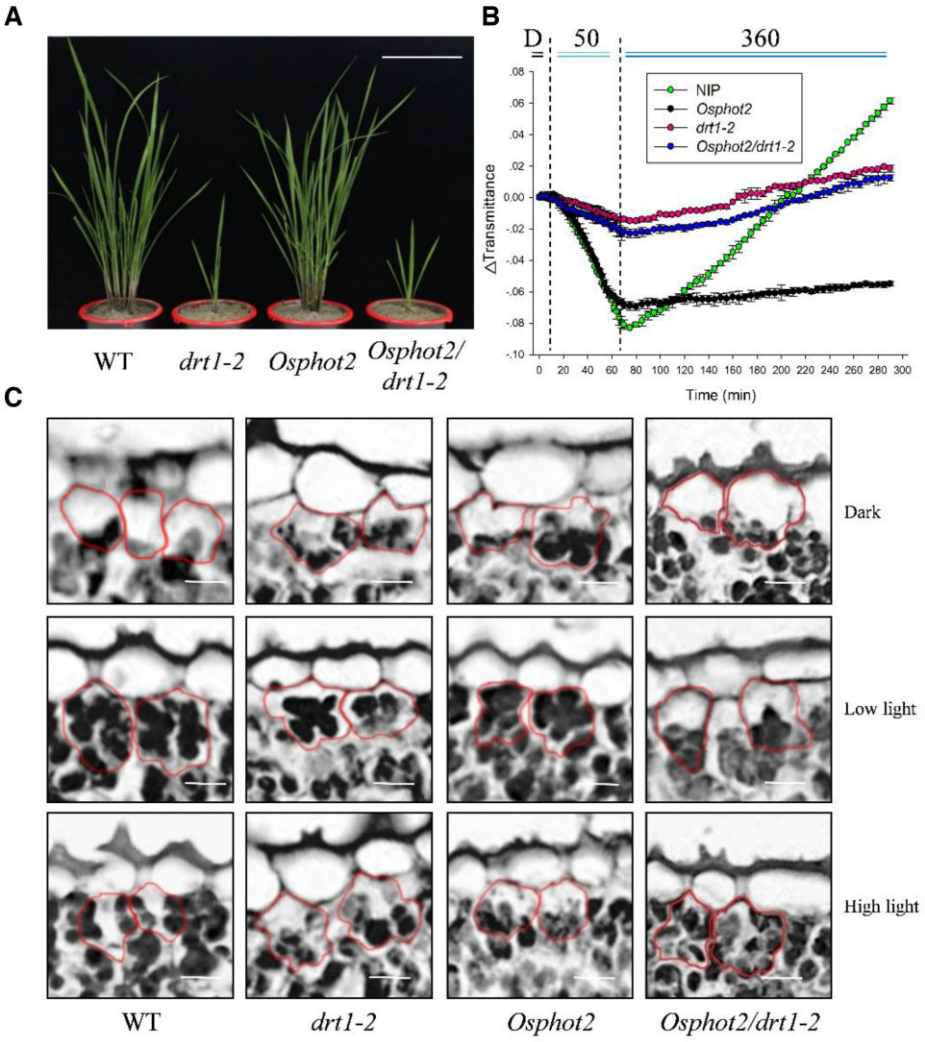

Figure 8 DRT1 is involved in OsPHOT2-mediated CP relocation. A, Gross morphology of WT, *drt1-2*, *Osphot2*, and *drt1-2*/*Osphot2* plants. Scale bar = 20 cm. B, Transmittance assay to detect the CP relocation response in WT, *drt1-2*, *Osphot2*, and *Osphot2*/*drt1-2* plants. Values are presented as means ± SD (n = 3). D, dark; 50, weak blue light (50 μmol/m2/s); 360, stronger blue light (360 μmol/m2/s). C, Sectioning of fixed WT, *drt1-2*, *Osphot2*, and *drt1-2*/*Osphot2* leaves. All the CPs in the four plants were mainly at the cell bottom after incubating for 24 h in the dark; When under low light, CP in WT and *Osphot2* moved to both upper and lower cell surfaces while the CPs in *drt1* and the double mutant remained at the bottom; Most CPs were on both sides of the mesophyll cells under high light in WT, but CPs mostly stay at the bottom in *drt1*, *Osphot2*, and double mutant. Scale bar = 10 μm.

However, inconsistent results regarding formin localizations also were reported. For example, as the first cloned Class I formin in Arabidopsis, AtFH5 was initially found on cell plate (Ingouff et al., 2005), but the recent results suggested that it was localized on plasmodesmata (Diao et al., 2018) or vesicle (Liu et al., 2018); Diao et al. also found, AtFH2, AtFH9, OsFH8, OsFH11, OsFH15, and OsFH16 were plasmodesmata-localized (Diao et al., 2018). Additionally, the AtFH4 was reported to be accumulated within the ER by transiently transformed *N. benthamiana* epidermal cells (Deeks et al., 2010). AtFH1 was found to translocate between PM, plasmodesmata, endosomes, and the tonoplast (Oulehlova et al., 2019). Here, we demonstrated that the Class I formin DRT1/OsFH13 binds with the PM (Figure 5). Moreover, the PM-localized DRT1 seemed to move from the PM onto the CP outer membrane peripherally upon light stimulation (Figure 7). This is partly supported by a previous investigation that OsFH5 is localized on the CP surface (Zhang et al., 2011). Thus, our study reports that formin protein can move upon light stimulus. These results suggested that the proper subcellular position of formins might be affected by the surrounding environment and developmental stages. Of course, it is also possible that other domains on formin may cooperate with the transmembrane domain to govern the subcellular localization of formin. However, it is still unknown whether OsFH5 is also a relocation protein. Therefore, it is interesting to explore whether other formins also have the relocation feature.

DRT1 is required for OsPHOT2-mediated CP avoidance response

In Arabidopsis, phototropins are associated with the PM in the dark and relocated in a blue-light-dependent manner (Sakamoto and Briggs, 2002; Kong et al., 2006). It has also been reported that modified AtPHOT1, which is permanently bound to the PM, is fully functional in the AtPHOT1-mediated physiological response, including CP relocation (Preuten et al., 2015). Moreover, the internalization of AtPHOT1 from the PM into the cytoplasm upon light stimulation may occur via clathrin-mediated endocytosis (Sakamoto and Briggs, 2002; Kaiserli et al., 2009). Recently, Ishishita et al. revealed that AtPHOT2 localized at the interface between the PM and the CPs is required for the CP avoidance response and possibly for stomatal opening as well (Ishishita et al., 2020). In contrast to the studies of phototropins in Arabidopsis, the knowledge about rice phototropins is limited. Here, we demonstrated that OsPHOT2 interacted with DRT1 (Figure 6). Moreover, we found that DRT1 is required for OsPHOT2 internalization because, in the *drt1* cells, the OsPHOT2 internalization was attenuated (Figure 7; Supplemental Figure S11). Previously, Kaiserli et al. revealed that clathrin might function in AtPHOT1 endocytic recruitment with pharmacological interference and coimmunoprecipitation assay (Kaiserli et al., 2009). Therefore, this evidence presumed that AtPHOT1 is trafficked through the endosomal recycling pathway. Similarly, Kong et al. found that AtPHOT2 accumulated in the so-called "BFA compartment" in the presence of BFA during the blue light stimulus, indicating that AtPHOT2 internalized in the endosomal recycling pathway (Kong et al., 2006). In Arabidopsis, cytoskeleton filament disassembly induced by drugs such as latrunculin B fully blocks CP relocation (Kandasamy and Meagher, 1999). Cp-actin filaments likely also play a pivotal role in CP relocation (Kadota et al., 2009; Suetsugu et al., 2010). In our study, we find the deficiency of DRT1 impaired microfilament organization (Figure 3), OsPHOT2 internalization (Figure 7) as well as CP relocation (Figure 8), suggesting that DRT1 cooperated with OsPHOT2 to regulate CP relocation. The heredity investigation assay further revealed that the microfilament network established by DRT1 might contribute to OsPHOT2 internalization and OsPHOT2-mediated CP relocation (Figures 7 and 8). Because OsPHOT2 is a kinase and one putative purpose of OsPHOT2 transporting is to phosphorylate its substrates on specific subcellular organelles (Kong et al., 2006). An intriguing possibility is that DRT1 might be a substrate of OsPHOT2, as it has several potential phosphorylation sites predicted at NetPhos 3.1 Server (http://www.cbs.dtu.dk/services/NetPhos-3.1/; Blom et al., 2004; Supplemental Figure S2).

Based on the present findings, we propose a model in which DRT1 regulates plant growth and CP photorelocation movement. On the one hand, DRT1 affects cell elongation, branch number, and seed size by altering the cytoskeleton; On the other hand, DRT1 interacts with OsPHOT2 to comigrate to CP to regulate CP movement under intense light, so as to reduce the damage caused by strong light (Supplemental Figure S13). The mechanisms underlying DRT1-mediated CP relocation warrant further study and may ultimately be an informative guide for breeding environmentally adapted high-yield crops.

Materials and methods

Plant materials and growth conditions

Seeds were sown after immersion for 2 d in darkness. The uniformly germinated seeds were sown in bottomless 96-well PCR plates with appropriate spacing in a nutrient solution. Rice (*O. sativa*) seedlings were grown at 30°C in a growth chamber under white light at an ~50 μmol m^{-2} s^{-1} (14 h)/dark (10 h) cycle (Chen et al., 2021). The mutant *drt1* was identified from a mutagenized population of rice ssp. Indica cv. Shuhui 527 (short to SH thereafter) mature seeds treated with EMS. The mutant stably inherited for multiple generations was applied for further experiments. Rice plants were grown in an experimental field at the China National Rice Research Institute, Hangzhou, under natural conditions.

Map-based cloning

To map the *DRT1* locus, the *drt1* mutant was crossed to Nipponbare (Japonica, shortened to NIP). A total of 5,392 individual F2 mutant plants were used for genetic mapping. To fine-map *DRT1*, four simple sequence repeat and eight sequence tag site markers were generated. The *DRT1* locus was delimited to a 74.3-Kb DNA region. The *drt1* mutation was identified by PCR amplifying the *DRT1* genomic region from SH and *drt1* mutant plants, followed by sequencing (Supplemental Table S4). The *drt1* mutant is also identified by restriction enzyme Hpy188I after PCR amplification of the *DRT1* genomic region from SH and *drt1* mutant plants with primers YP4736 and YP4737 (Supplemental Table S4). PCR products were digested or not with Hpy188I restriction enzyme at the mutation site for mutant and WT.

Vector construction and mutant creation

The *drt1-2* and *drt1-3* plants were generated using CRISPR/Cas9 as described previously (Wang et al., 2017) by the Biogle Company (Hangzhou, China). The sgRNA of *DRT1*: SG5789: 5′-CGAGAGTCCCTAGCGATGTCGGG-3′ was selected as the target. The sgRNA was created in the BGK03 vector containing Cas9 and then introduced into Nipponbare rice calli by Agrobacterium (EHA105)-mediated transformation. Eight independent lines of SG5789 were obtained. To examine the function of CRISPR/Cas9 in vivo, genomic DNA was extracted from transgenic plants and amplified by PCR for sequencing analysis (Supplemental Table S4) and used for further investigation.

Similarly, the *Osphot2* mutant was obtained using the CRISPR/Cas9 method, and the target sequence is 5′-CTGCTCAACTACCGCAAGGA-3′. Ten independent lines were obtained and were used in further investigation. Genomic DNA was extracted from transgenic plants and amplified by PCR for sequencing analysis (Supplemental Table S4).

For complementation analysis of the *drt1* mutant, a 10-Kb genomic fragment was amplified from WT. The PCR product was cloned into pCAMBIA1301 to generate the pCAM-DRT1 construct and was verified by sequencing. The resulting plasmid was transformed into calli derived from the *drt1* mutant using *A. tumefaciens* strain EHA105. Fifteen independent lines were obtained.

RNA extraction and RT-qPCR

Total RNA was extracted using TRIZOL reagent (Invitrogen, Waltham, MA, USA) according to the manufacturer's instructions. The first strand of cDNA was synthesized using PrimeScriptTMRT reagent Kit with gDNA Eraser (TaKaRa, Shiga, Japan), and RT-qPCR was performed using SYBR Premix (TaKaRa). The relative expression level of a target gene was normalized to that of rice ACTIN1 (LOC_Os03g50885). All primers used in RT-qPCR are listed in Supplemental Table S4.

Histochemical staining for GUS

To construct *DRT1p::GUS*, the 2,022 bp promoter was amplified by PCR using primer pair pGUS-F and pGUS-R and inserted into the pCAMBIA1301 vector. The vector was transformed into NIP rice. Samples were permeabilized in 90% (v/v) acetone for 1 h at −20°C and then washed twice with 0.01M PBS buffer before keeping in a vacuum for 5 min. And lastly, the samples were incubated with X-gluc at 37°C for 3–5 h. The green tissues were then de-colored with ethanol. For cross-sections, samples of leaves, roots, and coleoptiles were fixed in FAA (Formalin-acetic acid-alcohol) for 24 h at 4°C and cut into 8-μm-thick sections. The GUS staining images were taken using a Leica Light microscope (Liu et al., 2016).

Fusion protein purification and antibody production

The GFP fragment was amplified from pGA3427 (Kim et al., 2009), digested with EcoRV and BglII, and then inserted into pET30a to generate a pET30a-GFP vector. The *DRT1FH1FH2* and *DRT1FH2* fragments were amplified from DRT1 cDNA. EcoR V and BamH I were used to digest the fragments, which were then inserted individually into pET30a-GFP expression vectors for protein expression in the *Escherichia coli* BL21 (DE3) strain. Similarly, *FH1*, *FH2*, and *FH1FH2* fragments were inserted separately into pGEX-6P-1 (glutathione S-transferase fusion vectors). *LOV1*, *LOV2*, and *STK* fragments were inserted individually into pET30a. Cells containing these vectors separately were grown to an OD600 of 0.6 at 37°C and induced with 0.2 mmol/L Isopropyl β-D-Thiogalactoside at 22°C overnight. Cultures were collected by centrifugation and resuspended in binding buffer (40 mM PBS, pH 7.4). HIS-tagged proteins were purified using a Ni-NTA His bind resin, and GST-tagged proteins were purified using a GST-sefinose resin. Protein concentrations were determined using the Bradford reagent (Bio-Rad, Hercules, CA, USA) and bovine serum albumin (BSA) as a standard (Zhang et al., 2011).

A polyclonal antibody against DRT1 was raised in the rabbit at Hangzhou HuaAn Biotechnology Co., Ltd. Initial immunization was done with 500 mg of a polypeptide (RQHRSPPPSSTASC), and subsequent three-boost injections were done with 250 mg polypeptide for each injection. Polyclonal antibody against OsPHOT2 was raised in the rabbit at Wuhan Genecreate Biological Engineering Co., Ltd. The initial immunization was done with 200 mg of purified LOV1-HIS protein, and 100 mg for subsequent injections. The antibodies were used at a 1:300 dilution for western blotting.

Immunoblot experiments

Rice seedlings of the indicated age were harvested and ground to a fine powder in liquid nitrogen, followed by protein extraction in an extraction buffer containing 50 mM Tris pH 6.8, 4% (w/v) SDS, 10% (v/v) glycerol, 5% (v/v) 2-mercaptoethanol, 20% (w/v) bromophenol blue, a complete protease inhibitor (Sigma, St. Louis, MO, USA). Cellular debris was removed by centrifugation, and total protein concentration was quantified by Bradford assay and BSA as a standard. Proteins were separated by 10% SDS-PAGE and then transferred to nitrocellulose for immunoblotting experiments. Nitrocellulose membrane was blocked with 3% milk in TBST (0.8% (w/v) NaCl, 0.02% (w/v) KCl, 0.3% (w/v) Tris, pH 7.4, 0.05% (v/v) Tween20) for 30 min at room temperature. Excess milk was washed off with TBST. Blots were incubated in primary antibodies overnight at 4°C. Secondary antibodies were then applied for 1 h at room temperature. Blots were developed using the ECL solutions (Invitrogen).

Actin binding assay

The in vitro actin binding assay was performed according to the previously described methods with minor modifications (Barrero et al., 2002). GFP-HIS and FH1FH2-GFP-HIS obtained previously were mixed with rabbit monomeric actin (Sigma), followed by absorption using Ni-NTA His bind beads. After several washes of beads, the eluted protein samples were subjected to the protein gel blot analysis described above.

Ultraviolet absorption spectra of actin polymerization

The effects of DRT1FH1FH2 on rabbit muscle actin polymerization in vitro were analyzed by using ultraviolet absorption spectrum measurement according to Ren et al. (1997). G-actin from rabbit was added to the incubation buffer (PBS, pH = 7.5, 0.2 mmol/L ATP, 5 mmol/L $MgCl_2$, 0.1 mol/L KCl) to a concentration of 4 μmol/L and then incubated at 4°C for 2 h. After incubation, GFP-HIS, FH1FH2-GFP-HIS (50 nm) and FH1FH2-GFP-HIS (200 nm) were separately added. The absorption of G-actin solution at 232 nm was measured every 10 s by spectrophotometer for 30 min.

Actin filament binding assay

G-actin and actin filaments (3 μM) were incubated with 1 μM FH1FH2-GFP at room temperature for 1 h, and then

labeled with 3 μM Alexa Fluor 561-phalloidin (Invitrogen). Actin filaments were subsequently diluted to a final concentration of 10 nM in fluorescence buffer (10 mM imidazole, pH 7.0, 50 mM KCl, 2 mM $MgCl_2$, 1 mM EGTA, 100 mM DTT, 100 μg/mL glucoxidase, 15 mg/mL glucose, 20 μg/mL catalase and 0.5% (w/v) methylcellulose), modified from a previous study. The diluted samples were visualized using a Zeiss inverted fluorescence microscope (Axio Observer Z1) with a Zeiss plan-Apochromat 100x oil immersion objective (NA = 1.4; Tian et al., 2015).

Fluorescence microscopy of actin filaments and F-actin quantification

For observation of actin filaments, SH and *drt1* rice grains were germinated in a culture dish with distilled water for 4 d in darkness at 37°C. To avoid F-actin disruption in root hairs, the whole seedlings were fixed and vacuum-infiltrated for the first 5 min in a freshly prepared solution of 4% (w/v) paraformaldehyde in PEM buffer (100 mM PIPES, 10 mM EGTA, 0.3 M mannitol, 5 mM Mg_2SO_4, pH = 6.9), and then maintained for 1 h at 4°C. After three washes with PEM buffer, root hairs about 5 mm long were cut and incubated in 60 μL of 5 μM Alexa Fluor 488-Phalloidin in PEM buffer, then kept in the dark for 2 h at room temperature. After three PEM washes, the samples were observed in 50% (v/v) glycerol using a Zeiss LSM710 confocal laser scanning microscope. GFP fluorescence was observed after excitation using a 488-nm laser and detected using the bandpass 505–530 nm emission filter setting. F-actin was stained using the glycerol method to label pollen grains and cells in the elongation zone. Briefly, roots from 7-d-old seedlings and fresh mature pollen grains were incubated directly in PEM buffer containing 2% (v/v) glycerol and 5 μM Alexa Fluor 488-Phalloidin for 2 h, and then observed in 50% (v/v) glycerol after three washes. All images were analyzed with ImageJ software (Ye et al., 2009). The average pixel fluorescence intensity was obtained with ImageJ, then was plotted and analyzed in Microsoft Office Excel. Ten images for WT and *drt1* each were observed (Sun et al., 2017).

Subcellular localization

The coding sequences of *DRT1* and *OsPHOT2* were amplified by PCR and separately inserted into the pENTR/D-Topo donor vector using Gateway expression vector pGWB405 and pGWB541 (Nakagawa et al., 2007). The constructs were transiently expressed in protoplasts from SH cell suspensions by PEG-mediated transformation as described previously (Chen et al., 2016). For *N. benthamiana*, the recombinant vector and the control vector p35S-GFP were transformed into *Agrobacterium* (GV3101), which were injected into the *N. benthamiana* leaves. The leaves were then incubated in the darkness for 2–3 d and in weak light for 6 h. Pieces were cut and removed from some of the affected leaves and were used to prepare slides (Wang et al., 2019).

For the light-dependent dissociation experiment, the protoplasts were kept in darkness before detection using a confocal laser scanning microscope (LSM 710, Zeiss, Germany). GFP fluorescence was observed after excitation using a 488-nm laser and detected using the bandpass 505–530 nm emission filter setting. CFP was observed after excitation using a 436-nm and detected using the bandpass 470-495 nm emission filter setting. RFP was observed after excitation using a 561-nm and detected using the bandpass 605–630 nm emission filter setting. For LatB treatment, the protoplasts were treated with 100 nM LatB for 30 min before detection (Qu et al., 2020). All images were analyzed with ImageJ software.

CP and CP subfraction isolation

Intact CPs were isolated and resuspended from 4-week-old SH seedlings as described previously (Kong et al., 2013). The resuspended CPs were used for CP subfraction isolation as described previously (Chen et al., 2016). To determine the DRT1 localization in CPs, immunoblot analysis was performed with isolated CPs treated with thermolysin (100 and 200 μg/mL) for 20 min on ice.

Yeast two-hybrid assay

The binding domain and activation domain plasmids containing the DRT1 and OsPHOT2 sequences were constructed by subcloning the coding sequences into the pGBKT7 and pGADT7 vectors. The bait and prey plasmids were transformed into the yeast strain AH109. To analyze protein interaction, yeast colonies were patched in duplicate onto SD-T-L, and SD-T-L-H plates, then incubated at 30°C for 2–3 d.

LCI assay

The coding sequences of DRT1FH1FH2 and OsPHOT2 were amplified and cloned into the pCAMBIA1300-nLUC and pCAMBIA1300-cLUC vectors, respectively. *Agrobacterium tumefaciens* (GV3101) bacteria containing the constructs were grown in the YEB medium at 28°C overnight, pelleted, and resuspended to OD600 = 0.3 in the induction medium. The culture was grown in an induction medium for 8–12 h. The bacteria were washed once with MS medium containing 10 mM MES, pH 5.6, and resuspended in Murashige and Skoog (MS)-MES medium containing 150 μM acetosyringone to a final concentration of OD600 = 0.5. The bacterial suspension was mixed and infiltrated into *N. benthamiana* leaves, which were subsequently covered with plastic for 2 d and recovered to light for 16 h. A low-light cooled CCD imaging apparatus (ROPER CA2048B; ROPER Scientific) was used to capture the LUC images (Chen et al., 2008).

Co-immunoprecipitation assay

The co-immunoprecipitation assay was performed according to previously described methods (Moffett et al., 2002). Full-length *DRT1* and *OsPHOT2* were amplified and inserted into pGWB405 and pGWB414 vectors, respectively. The resulting transient expression constructs were transformed into GV3101, and Agroinfiltrations were performed as described above. After incubation for 2 d, proteins were extracted with extraction buffer [25 mM Tris–HCl, pH 7.5, 1 mM EDTA,

150 mM NaCl, 10% glycerol, 5 mM dithiothreitol] in the presence of protease inhibitor cocktail (Sigma). Their interaction was detected by an anti-OsPHOT2 antibody.

In vitro pull-down assay

For the pull-down assay, roughly equal amounts of purified GST, GST-FH1, GST-FH2, GST-FH1FH2, and GST-FH1FH2 (MT) fusion proteins were affixed to GST-sefinose resin and then incubated with LOV1-HIS, LOV2-HIS, or STK-HIS fusion proteins separately at 4°C for 1 h. The bound proteins were used for immunoblotting analysis using anti-His and anti-GST antibodies.

Analysis of CP movement

Red-light transmittances were measured using an ultraviolet-visible spectrometer according to a previously described protocol (Wen et al., 2012). Briefly, 8-week-old seedlings cultured in nutrient solution were dark-adapted for about 3 d. The blade was punched into small discs, followed by pouring 300 μL of 0.5% (w/v) gellan gum melted in 1/2 MS medium into each well of the 96-well enzyme label plates. The discs were placed adaxial side up at the center of the well. A transparent film was used to cover a hole on each well. After keeping in the dark for 3 h, the transmittance changes were recorded under the different light conditions of red light (660 nm) every 2 or 5 min. We used weak blue light (50 μmol/m^2/s, 75 min) to measure the CP accumulation response (Ac) and stronger blue light (360 μmol/m^2/s, 215 min) for the avoidance response (Av). A blue light-emitting diode illuminator (RBIRWG150; JIUPO) was used to generate blue light. For confocal microscopy, 2-week-old seedlings cultured in nutrient solution were dark-adapted for about 24 h and then irradiated with white light at 50 or 300 μmol/m^2/s for 2 h. Leaves of dark-adapted and white light-treated plants were cut and fixed with 2.5% glutaraldehyde. Specimens were observed and photographed using the spontaneous fluorescence of CPs under a microscope at 568 nm, as described by Wada (2013). For cross sections, 2-week-old seedlings cultured in nutrient solution were dark-adapted for about 24 h, and then irradiated with blue light at 50 or 300 μmol/m^2/s for 2 h. Leaves of dark-adapted and blue light-treated plants were cut and fixed with 2.5% glutaraldehyde in fixation buffer (20 mM PIPES, 5 mM $MgCl_2$, 5 mM EGTA, 0.5 mM phenylmethylsulfonyl fluoride, 1% dimethyl sulfoxide, pH 7.0). Then embedded in Spur's resin and sectioned using a Reichert ultramicrotome. The sections were stained with toluidine blue. Specimens were observed and photographed under a microscope.

PM protein and organelle protein fractionation

PM protein and organelle protein fractionation were performed according to previously described methods (Shen et al., 2017). They were extracted by a Minute PM Protein Isolation Kit for Plants (Invent Biotechnologies). Immunoblot analysis was performed using antibodies against Actin (total protein marker), RbcL (chloroplast marker), H^+-ATPase (plasma membrane marker), OsPHOT2, and DRT1.

Sequences analysis

Sequences of DAA63388 (*Z. mays*), XP_003560022 (*B. distachyon*), and DRT1 were aligned by using Clustal Omega (https://www.ebi.ac.uk/Tools/msa/clustalo/) and then the Multiple-Alignment file was shaded by ExPASy (https://embnet.vital-it.ch/software/BOX_form.html). The physicochemical properties and posttranslational modifications, such as phosphorylation sites, were predicted at ExPASy Protein (www.expasy.org).

Accession numbers

Sequence data from this article can be found in the GenBank/EMBL data libraries under accession numbers: *DRT1*, LOC_Os07g39920; *OsPHOT2*, LOC_Os04g23890; *OsRAC*, LOC_Os01g12900; *Actin*, LOC_Os03g50885.

Supplemental data

The following materials are available in the online version of this article.

Supplemental Figure S1. *drt1* mutants display morphological defects.

Supplemental Figure S2. DRT1 protein sequence alignment.

Supplemental Figure S3. Knockout mutant *drt1-2* and *drt1-3* present similar phenotype with *drt1*.

Supplemental Figure S4. DRT1 expression pattern analysis.

Supplemental Figure S5. Microfilament organization in RE#1, *drt1-2* and *drt1-3* plants.

Supplemental Figure S6. Subcellular Localization of the DRT1 protein.

Supplemental Figure S7. Coomassie blue staining for recombinant proteins.

Supplemental Figure S8. Generation of the *Osphot2* mutant by CRISPR/Cas9.

Supplemental Figure S9. The *Osphot2* mutant exhibits impaired CP relocation.

Supplemental Figure S10. Subcellular localization of the DRT1 protein.

Supplemental Figure S11. The distribution and relocation feature of free GFP protein and OsPHOT2 in protoplasts.

Supplemental Figure S12. The observation of CP position by confocal microscope.

Supplemental Figure S13. A model summarizing the regulatory mechanism of DRT1 in plant development and CP photorelocation movement.

Supplemental Table S1. A single recessive nuclear locus controls drt1 phenotype.

Supplemental Table S2. Agronomic characters in WT, *drt1* mutant, RE#1 and RE#2.

Supplemental Table S3. Agronomic characters in NIP, *drt1-2* and *drt1-3*.

Supplemental Table S4. A list of primers used in this study.

Acknowledgments

We thank Dr. Lixin Zhang and Dr. Lianwei Peng (Chinese Academy of Sciences) for kindly gifting all of the photosynthetic antibodies.

Funding

This work was supported by Funds from Error! Hyperlink reference not valid. (91335103, 91735303, 31271696, and 31901481), the Natural Science Foundation of Zhejiang (LY20C130004 and LGN19C130006).

Conflict of interest statement. None declared.

References

Bao L, Inoue N, Ishikawa M, Gotoh E, Teh OK, Higa T, Morimoto T, Ginanjar EF, Harashima H, Noda N, et al. (2022) A PSTAIRE-type cyclin-dependent kinase controls light responses in land plants. Sci Adv **8**: eabk2116

Barrero RA, Umeda M, Yamamura S, Uchimiya H (2002) Arabidopsis CAP regulates the actin cytoskeleton necessary for plant cell elongation and division. Plant Cell **14**: 149–163

Blom N, Sicheritz-Ponten T, Gupta R, Gammeltoft S, Brunak S (2004) Prediction of post-translational glycosylation and phosphorylation of proteins from the amino acid sequence. Proteomics **4**: 1633–1649

Chang S, Ren Z, Liu C, Du P, Li J, Liu Z, Zhang F, Hou H, Shi J, Liang W, et al. (2021) OsFH3 encodes a type II formin required for rice morphogenesis. Int J Mol Sci **22**: 13250

Chen F, Dong G, Wang F, Shi Y, Zhu J, Zhang Y, Ruan B, Wu Y, Feng X, Zhao C, et al. (2021) A beta-ketoacyl carrier protein reductase confers heat tolerance via the regulation of fatty acid biosynthesis and stress signaling in rice. New Phytol **232**: 655–672

Chen F, Dong G, Wu L, Wang F, Yang X, Ma X, Wang H, Wu J, Zhang Y, Wang H, et al. (2016) A nucleus-encoded chloroplast protein YL1 is involved in chloroplast development and efficient biogenesis of chloroplast ATP synthase in rice. Sci Rep **6**: 32295

Chen H, Zou Y, Shang Y, Lin H, Wang Y, Cai R, Tang X, Zhou JM (2008) Firefly luciferase complementation imaging assay for protein-protein interactions in plants. Plant Physiol **146**: 368–376

Cheung AY, Wu HM (2004) Overexpression of an Arabidopsis formin stimulates supernumerary actin cable formation from pollen tube cell membrane. Plant Cell **16**: 257–269

Cifrova P, Oulehlova D, Kollarova E, Martinek J, Rosero A, Zarsky V, Schwarzerova K, Cvrckova F (2020) Division of labor between two actin nucleators-the formin FH1 and the ARP2/3 complex-in Arabidopsis epidermal cell morphogenesis. Front Plant Sci **11**: 148

Cvrckova F (2013) Formins and membranes: anchoring cortical actin to the cell wall and beyond. Front Plant Sci **4**: 436

Cvrckova F, Novotny M, Pickova D, Zarsky V (2004) Formin homology 2 domains occur in multiple contexts in angiosperms. BMC Genomics **5**: 44

Deeks MJ, Cvrckova F, Machesky LM, Mikitova V, Ketelaar T, Zarsky V, Davies B, Hussey PJ (2005) Arabidopsis group Ie formins localize to specific cell membrane domains, interact with actin-binding proteins and cause defects in cell expansion upon aberrant expression. New Phytol **168**: 529–540

Deeks MJ, Fendrych M, Smertenko A, Bell KS, Oparka K, Cvrckova F, Zarsky V, Hussey PJ (2010) The plant formin AtFH4 interacts with both actin and microtubules, and contains a newly identified microtubule-binding domain. J Cell Sci **123**: 1209–1215

Diao M, Ren S, Wang Q, Qian L, Shen J, Liu Y, Huang S (2018) Arabidopsis formin 2 regulates cell-to-cell trafficking by capping and stabilizing actin filaments at plasmodesmata. Elife **7**: e36316

Favery B, Chelysheva LA, Lebris M, Jammes F, Marmagne A, De Almeida-Engler J, Lecomte P, Vaury C, Arkowitz RA, Abad P (2004) Arabidopsis formin AtFH6 is a plasma membrane-associated protein upregulated in giant cells induced by parasitic nematodes. Plant Cell **16**: 2529–2540

Fu Y, Gu Y, Zheng Z, Wasteneys G, Yang Z (2005) Arabidopsis interdigitating cell growth requires two antagonistic pathways with opposing action on cell morphogenesis. Cell **120**: 687–700

Goode BL, Eck MJ (2007) Mechanism and function of formins in the control of actin assembly. Annu Rev Biochem **76**: 593–627

Grunt M, Zarsky V, Cvrckova F (2008) Roots of angiosperm formins: the evolutionary history of plant FH2 domain-containing proteins. BMC Evol Biol **8**: 115

Huala E, Oeller PW, Liscum E, Han IS, Larsen E, Briggs WR (1997) Arabidopsis NPH1: a protein kinase with a putative redox-sensing domain. Science **278**: 2120–2123

Huang G, Liang W, Sturrock CJ, Pandey BK, Giri J, Mairhofer S, Wang D, Muller L, Tan H, York LM, et al. (2018) Rice actin binding protein RMD controls crown root angle in response to external phosphate. Nat Commun **9**: 2346

Huang J, Kim CM, Xuan YH, Liu J, Kim TH, Kim BK, Han CD (2013) Formin homology 1 (OsFH1) regulates root-hair elongation in rice (*Oryza sativa*). Planta **237**: 1227–1239

Ingouff M, Fitz Gerald JN, Guerin C, Robert H, Sorensen MB, Van Damme D, Geelen D, Blanchoin L, Berger F (2005) Plant formin AtFH5 is an evolutionarily conserved actin nucleator involved in cytokinesis. Nat Cell Biol **7**: 374–380

Inoue Y, Shibata K (1973) Light-induced chloroplast rearrangements and their action spectra as measured by absorption spectrophotometry. Planta **114**: 341–358

Ishishita K, Higa T, Tanaka H, Inoue SI, Chung A, Ushijima T, Matsushita T, Kinoshita T, Nakai M, Wada M, et al. (2020) Phototropin2 contributes to the chloroplast avoidance response at the chloroplast-plasma membrane interface. Plant Physiol **183**: 304–316

Jarillo JA, Gabrys H, Capel J, Alonso JM, Ecker JR, Cashmore AR (2001) Phototropin-related NPL1 controls chloroplast relocation induced by blue light. Nature **410**: 952–954

Kadota A, Yamada N, Suetsugu N, Hirose M, Saito C, Shoda K, Ichikawa S, Kagawa T, Nakano A, Wada M (2009) Short actin-based mechanism for light-directed chloroplast movement in Arabidopsis. Proc Natl Acad Sci USA **106**: 13106–13111

Kaiserli E, Sullivan S, Jones MA, Feeney KA, Christie JM (2009) Domain swapping to assess the mechanistic basis of Arabidopsis phototropin 1 receptor kinase activation and endocytosis by blue light. Plant Cell **21**: 3226–3244

Kandasamy MK, Meagher RB (1999) Actin-organelle interaction: association with chloroplast in arabidopsis leaf mesophyll cells. Cell Motil Cytoskeleton **44**: 110–118

Kasahara M, Kagawa T, Oikawa K, Suetsugu N, Miyao M, Wada M (2002) Chloroplast avoidance movement reduces photodamage in plants. Nature **420**: 829–832

Kihara M, Ushijima T, Yamagata Y, Tsuruda Y, Higa T, Abiko T, Kubo T, Wada M, Suetsugu N, Gotoh E (2020) Light-induced chloroplast movements in Oryza species. J Plant Res **133**: 525–535

Kim SR, Lee DY, Yang JI, Moon S, An G (2009) Cloning vectors for rice. J Plant Biol **52**: 73–78

Kinoshita T, Doi M, Suetsugu N, Kagawa T, Wada M, Shimazaki K (2001) Phot1 and phot2 mediate blue light regulation of stomatal opening. Nature **414**: 656–660

Kollarova E, Baquero Forero A, Cvrckova F (2021) The *Arabidopsis thaliana* class II formin FH13 modulates pollen tube growth. Front Plant Sci **12**: 599961

Kong SG, Suetsugu N, Kikuchi S, Nakai M, Nagatani A, Wada M (2013) Both phototropin 1 and 2 localize on the chloroplast outer membrane with distinct localization activity. Plant Cell Physiol **54**: 80–92

Kong SG, Suzuki T, Tamura K, Mochizuki N, Hara-Nishimura I, Nagatani A (2006) Blue light-induced association of phototropin 2 with the Golgi apparatus. Plant J **45**: 994–1005

Kong SG, Wada M (2011) New insights into dynamic actin-based chloroplast photorelocation movement. Mol Plant **4**: 771–781

Kovar DR, Pollard TD (2004) Progressing actin: formin as a processive elongation machine. Nat Cell Biol **6**: 1158–1159

Li C, Wang Y, Liu L, Hu Y, Zhang F, Mergen S, Wang G, Schlappi MR, Chu C (2011) A rice plastidial nucleotide sugar epimerase is involved in galactolipid biosynthesis and improves photosynthetic efficiency. PLoS Genet **7**: e1002196

Li G, Yang X, Zhang X, Song Y, Liang W, Zhang D (2018) Rice morphology determinant-mediated actin filament organization contributes to pollen tube growth. Plant Physiol **177**: 255–270

Lian N, Wang XW, Jing YP, Lin JX (2021) Regulation of cytoskeleton-associated protein activities: linking cellular signals to plant cytoskeletal function. J Integr Plant Biol **63**: 241–250

Liu C, Zhang Y, Ren H (2018) Actin polymerization mediated by AtFH5 directs the polarity establishment and vesicle trafficking for pollen germination in Arabidopsis. Mol Plant **11**: 1389–1399

Liu C, Zhu H, Xing Y, Tan J, Chen X, Zhang J, Peng H, Xie Q, Zhang Z (2016) Albino Leaf 2 is involved in the splicing of chloroplast group I and II introns in rice. J Exp Bot **67**: 5339–5347

Liu J, Lu Y, Hua W, Last RL (2019) A new light on photosystem II maintenance in oxygenic photosynthesis. Front Plant Sci **10**: 975

Ma Z, Sun Y, Zhu X, Yang L, Chen X, Miao Y (2021) Membrane nanodomains modulate formin condensation for actin remodeling in Arabidopsis innate immune responses. Plant Cell **34**: 374–394

Michelot A, Derivery E, Paterski-Boujemaa R, Guerin C, Huang S, Parcy F, Staiger CJ, Blanchoin L (2006) A novel mechanism for the formation of actin-filament bundles by a nonprocessive formin. Curr Biol **16**: 1924–1930

Michelot A, Guerin C, Huang S, Ingouff M, Richard S, Rodiuc N, Staiger CJ, Blanchoin L (2005) The formin homology 1 domain modulates the actin nucleation and bundling activity of Arabidopsis FORMIN1. Plant Cell **17**: 2296–2313

Moffett P, Farnham G, Peart J, Baulcombe DC (2002) Interaction between domains of a plant NBS-LRR protein in disease resistance-related cell death. EMBO J **21**: 4511–4519

Nakagawa T, Kurose T, Hino T, Tanaka K, Kawamukai M, Niwa Y, Toyooka K, Matsuoka K, Jinbo T, Kimura T (2007) Development of series of gateway binary vectors, pGWBs, for realizing efficient construction of fusion genes for plant transformation. J Biosci Bioeng **104**: 34–41

Nishiyama Y, Murata N (2014) Revised scheme for the mechanism of photoinhibition and its application to enhance the abiotic stress tolerance of the photosynthetic machinery. Appl Microbiol Biotechnol **98**: 8777–8796

Ono E, Wong HL, Kawasaki T, Hasegawa M, Kodama O, Shimamoto K (2001) Essential role of the small GTPase Rac in disease resistance of rice. Proc Natl Acad Sci USA **98**: 759–764

Oulehlova D, Kollarova E, Cifrova P, Pejchar P, Zarsky V, Cvrckova F (2019) Arabidopsis class I formin FH1 relocates between membrane compartments during root cell ontogeny and associates with plasmodesmata. Plant Cell Physiol **60**: 1855–1870

Perico C, Sparkes I (2018) Plant organelle dynamics: cytoskeletal control and membrane contact sites. New Phytol **220**: 381–394

Preuten T, Blackwood L, Christie JM, Fankhauser C (2015) Lipid anchoring of Arabidopsis phototropin 1 to assess the functional significance of receptor internalization: should I stay or should I go? New Phytol **206**: 1038–1050

Qu XL, Wang QN, Wang HY, Huang SJ (2020) Visualization of actin organization and quantification in fixed Arabidopsis pollen grains and tubes. Bio-Protocol **10**: e3509

Ren H, Gibbon BC, Ashworth SL, Sherman DM, Yuan M, Staiger CJ (1997) Actin purified from maize pollen functions in living plant cells. Plant Cell **9**: 1445–1457

Rosero A, Oulehlova D, Stillerova L, Schiebertova P, Grunt M, Zarsky V, Cvrckova F (2016) Arabidopsis FH1 formin affects cotyledon pavement cell shape by modulating cytoskeleton dynamics. Plant Cell Physiol **57**: 488–504

Rosero A, Zarsky V, Cvrckova F (2017) AtFH1 formin mutation affects actin filament and microtubule dynamics in *Arabidopsis thaliana*. J Exp Bot **68**: 5979

Sakamoto K, Briggs WR (2002) Cellular and subcellular localization of phototropin 1. Plant Cell **14**: 1723–1735

Sakata M, Kimura S, Fujii Y, Sakai T, Kodama Y (2019) Relationship between relocation of phototropin to the chloroplast periphery and the initiation of chloroplast movement in *Marchantia polymorpha*. Plant Direct **3**: e00160

Schmidt von Braun S, Schleiff E (2008) The chloroplast outer membrane protein CHUP1 interacts with actin and profilin. Planta **227**: 1151–1159

Shang B, Zang Y, Zhao X, Zhu J, Fan C, Guo X, Zhang X (2019) Functional characterization of GhPHOT2 in chloroplast avoidance of *Gossypium hirsutum*. Plant Physiol Biochem **135**: 51–60

Shen Q, Bourdais G, Pan H, Robatzek S, Tang D (2017) Arabidopsis glycosylphosphatidylinositol-anchored protein LLG1 associates with and modulates FLS2 to regulate innate immunity. Proc Natl Acad Sci USA **114**: 5749–5754

Song Y, Li G, Nowak J, Zhang XQ, Xu DB, Yang XJ, Huang GQ, Liang WQ, Yang LT, Wang CH, et al. (2019) The rice actin-binding protein RMD regulates light-dependent shoot gravitropism. Plant Physiol **181**: 630–644

Suetsugu N, Higa T, Wada M (2017) Ferns, mosses and liverworts as model systems for light-mediated chloroplast movements. Plant Cell Environ **40**: 2447–2456

Suetsugu N, Sato Y, Tsuboi H, Kasahara M, Imaizumi T, Kagawa T, Hiwatashi Y, Hasebe M, Wada M (2012) The KAC family of kinesin-like proteins is essential for the association of chloroplasts with the plasma membrane in land plants. Plant Cell Physiol **53**: 1854–1865

Suetsugu N, Yamada N, Kagawa T, Yonekura H, Uyeda TQ, Kadota A, Wada M (2010) Two kinesin-like proteins mediate actin-based chloroplast movement in *Arabidopsis thaliana*. Proc Natl Acad Sci USA **107**: 8860–8865

Sun T, Li S, Ren H (2017) OsFH15, a class I formin, interacts with microfilaments and microtubules to regulate grain size via affecting cell expansion in rice. Sci Rep **7**: 6538

Tian J, Han L, Feng Z, Wang G, Liu W, Ma Y, Yu Y, Kong Z (2015) Orchestration of microtubules and the actin cytoskeleton in trichome cell shape determination by a plant-unique kinesin. Elife **4**: e09351

Wada M (2013) Chloroplast movement. Plant Sci **210**: 177–182

Wang J, Xue X, Ren H (2012) New insights into the role of plant formins: regulating the organization of the actin and microtubule cytoskeleton. Protoplasma **249**: S101–107

Wang J, Yu H, Xiong G, Lu Z, Jiao Y, Meng X, Liu G, Chen X, Wang Y, Li J (2017) Tissue-specific ubiquitination by IPA1 INTERACTING PROTEIN1 modulates IPA1 protein levels to regulate Plant Architecture in Rice. Plant Cell **29**: 697–707

Wang JJ, Zhang Y, Wu J, Meng L, Ren HY (2013) At FH16, an Arabidopsis type II formin, binds and bundles both microfilaments and microtubules, and preferentially binds to microtubules. J Integr Plant Biol **55**: 1002–1015

Wang P, Zhang S, Qiao J, Sun Q, Shi Q, Cai C, Mo J, Chu Z, Yuan Y, Du X, et al. (2019) Functional analysis of the GbDWARF14 gene associated with branching development in cotton. PeerJ **7**: e6901

Wang PW, Gao EL, Hussey PJ (2020) Autophagosome biogenesis in plants: an actin cytoskeleton perspective. Trends Plant Sci **25**: 850–858

Wang Y, Li J (2008) Molecular basis of plant architecture. Annu Rev Plant Biol **59**: 253–279

Wen F, Wang JQ, Xing D (2012) A protein phosphatase 2A catalytic subunit modulates blue light-induced chloroplast avoidance movements through regulating actin cytoskeleton in Arabidopsis. Plant Cell Physiol **53**: 1366–1379

Xie Y, Miao Y (2021) Polarisome assembly mediates actin remodeling during polarized yeast and fungal growth. J Cell Sci **134**: jcs247916

Xu C, Wang Y, Yu Y, Duan J, Liao Z, Xiong G, Meng X, Liu G, Qian Q, Li J (2012) Degradation of MONOCULM 1 by APC/C(TAD1) regulates rice tillering. Nat Commun **3**: 750

Xue XH, Guo CQ, Du F, Lu QL, Zhang CM, Ren HY (2011) AtFH8 is involved in root development under effect of low-dose latruncu-lin B in dividing cells. Mol Plant **4**: 264–278

Yang B, Tang J, Yu ZH, Khare T, Srivastav A, Datir S, Kumar V (2019) Light stress responses and prospects for engineering light stress tolerance in crop plants. J Plant Growth Regul **38**: 1489–1506

Yang W, Ren S, Zhang X, Gao M, Ye S, Qi Y, Zheng Y, Wang J, Zeng L, Li Q, Huang S, He Z (2011) BENT UPPERMOST INTERNODE1 encodes the class II formin FH5 crucial for actin organization and rice development. Plant Cell **23**: 661–680

Ye J, Zheng Y, Yan A, Chen N, Wang Z, Huang S, Yang Z (2009) Arabidopsis formin3 directs the formation of actin cables and polarized growth in pollen tubes. Plant Cell **21**: 3868–3884

Yi K, Guo C, Chen D, Zhao B, Yang B, Ren H (2005) Cloning and functional characterization of a formin-like protein (AtFH8) from Arabidopsis. Plant Physiol **138**: 1071–1082

Zhang L, Huang J, Wang Y, Xu R, Yang Z, Zhao Z, Liu S, Tian Y, Zheng X, Wang J, et al. (2020) Identification and genetic analysis of qCL1.2, a novel allele of the "green revolution" gene SD1 from wild rice (Oryza rufipogon) that enhances plant height. BMC Genet **21**: 62

Zhang Z, Zhang Y, Tan H, Wang Y, Li G, Liang W, Yuan Z, Hu J, Ren H, Zhang D (2011) RICE MORPHOLOGY DETERMINANT encodes the type II formin FH5 and regulates rice morphogenesis. Plant Cell **23**: 681–700

Zheng Y, Xin H, Lin J, Liu CM, Huang S (2012) An Arabidopsis class II formin, AtFH19, nucleates actin assembly, binds to the barbed end of actin filaments, and antagonizes the effect of AtFH1 on actin dynamics. J Integr Plant Biol **54**: 800–813